SURFACE ENERGY CHARACTERISTICS OF GRANITE AND LIMESTONE AGGREGATES WITH RESPECT TO 2D AND 3D SURFACE ROUGHNESS MEASUREMENTS

By

ANJANA THOROPPADY KITTU

Bachelor of Technology in Civil Engineering

Mahatma Gandhi University

Kottayam, Kerala

2007

Submitted to the Faculty of the
Graduate College of the
Oklahoma State University
in partial fulfillment of
the requirements for
the Degree of
MASTER OF SCIENCE
December, 2013

SURFACE ENERGY CHARACTERISTICS OF GRANITE AND LIMESTONE AGGREGATES WITH RESPECT TO 2D AND 3D SURFACE ROUGHNESS MEASUREMENTS

Thesis Approved:

Dr. Rifat Bulut

Thesis Adviser

Dr. Sandip S Harimkar

Dr. Avdesh Tyagi

.

ACKNOWLEDGEMENTS

I believe it as a great opportunity in my life to pursue a Master of Science in Civil Engineering from prestigious institution, Oklahoma State University, Stillwater. I use this opportunity to express my deepest gratitude to all concerned.

First and foremost, I would like to express my obligation and heartfelt indebtedness to my advisor, Dr. Rifat Bulut who gave me the wonderful opportunity to be the part of his research team. It was his knowledge, support and encouragement which motivated me through this research and my Masters program. I would like to express my grateful acknowledgement to Dr. Sandip Harimkar for his generous help in letting me use his lab facilities. His precious comments and kind co-operation helped me to complete one of the important parts of my thesis.

I am thankful to Dr. Avdesh Tyagi for serving as a member in my thesis committee.

I am using this opportunity to thank Dr. Jim Puckette for helping me with sample preparation, for letting me use his lab equipments as well as for providing precious comments and suggestions. I would like to thank my fellow labmates Murat and Aditya for helping me in several stages of my research. With great fondness, I express my feelings of gratefulness to my friends Sruthi and Spandana for their love and support. Further, I would extend thanks to Omar and Chen for all their help in making the final semester of my Masters program less stressful.

No words are enough to express my thanks to my husband and my loving daughter for providing motivation and support to me, whenever I hit a rough patch. I thankfully remember all my family members on this occasion. I use this opportunity to extend my thanks to Oklahoma Department of Transportation and Oklahoma Transportation Center for the funding provided for this study. Last but not least, I bow before Almighty for all the blessing showered upon me.

Name: ANJANA THOROPPADY KITTU

Date of Degree: DECEMBER, 2013

Title of Study: SURFACE ENERGY CHARACTERISTICS OF GRANITE AND LIMESTONE AGGREGATES WITH RESPECT TO 2D AND 3D SURFACE ROUGHNESS MEASUREMENTS

Major Field: CIVIL ENGINEERING

Abstract: Surface energy properties of aggregates and asphalt binders can be used to select appropriate aggregate and asphalt binder combinations for the construction of moisture durable pavements. Sessile drop device is an effective method to determine the surface properties of aggregates and asphalt binders by performing direct contact angle measurements. However, the variations in surface roughness could impact the contact angle formed on the aggregate surface. Therefore, the present study was intended to evaluate the contact angle measurements on aggregate surfaces at different levels of surface roughness using the sessile drop device. Large size granite and limestone rock specimens were obtained and cut into appropriate sizes to create flat surfaces for contact angle measurements. The samples were subjected to a series of polishing stages using different particle sizes of silicon carbide and aluminum oxide grits. Contact angle measurements were subsequently conducted using three probe liquids on the unpolished surface as well as on the specimens subjected to different levels of polishing. Surface roughness measurements were also performed after each polishing stage using a two-dimensional profilometer and a three dimensional optical profilometer. The surface roughness decreased as the polishing progressed. The results from this study showed that as the surface became smoother, the values of contact angles formed by the probe liquids decreased, and attained consistent values after polishing with silicon carbide 1000 grit. The surface energy components also showed consistent results from the silicon carbide 1000 polishing stage onwards. Present results imply that initial polishing of aggregate surface is required to obtain consistent results from the sessile drop device. Correlation between two methods of measurements of surface roughness indicates that both methods could be useful for measurement of rock samples. Once the surface roughness is standardized to obtain representative contact angle, the sessile drop device can be used to compare different aggregates and select appropriate aggregate-asphalt binder combination for the construction of durable pavements. The surface energy results obtained from the contact angle measurements were used to evaluate the energy ratio and the compatibility ratio parameters for moisture damage potential of the two aggregate-binder combinations along with PG 64-22 neat binder. The results obtained indicate that ER and CR could be used as power tools for material selection.

TABLE OF CONTENTS

Chapter Page

LIST OF TABLES

Table Page

LIST OF FIGURES

Figure Page

CHAPTER I

INTRODUCTION

1.1 Problem Statement

In the United States, almost 94% of the paved roads are surfaced with asphalt (NAPA, 2013) which contributes to about 18 billion tons of asphalt (APA, 2013). Based on the statistics from the National Surface Transportation Policy and Revenue Study Commission of the U.S. Congress, the nation is spending $68 billion/year for maintaining the highways, roads, and bridges nationwide and is estimated to be $185 billion/year over the next 50 years (APA, 2013). For that reason, there is an increasing demand for research which could ensure the longevity of asphalt pavements. The durability of asphalt pavement can be affected by traffic load on the pavement as well as various environmental factors. Various environmental factors include moisture (precipitation as well as ground water), changes in temperature, aging of the pavement etc. (Terrel and Al-Swailmi, 1994). Among these, moisture is a major contributor to the weakening of the asphalt mixture. Progressive damage of asphalt mixes due to loss of adhesion between the binder and aggregate surface and/or cohesion of asphalt in the presence of moisture is referred to as moisture damage. Three reasons for moisture damage are loss of cohesive energy of the asphalt, deterioration of the asphalt-aggregate adhesive strength and the degradation or fracture of the aggregate (Terrel and Al-Swailmi, 1994). Also, several studies have shown that the moisture damage resistance of asphalt mixes depend on the adhesive and cohesive strength between aggregate and asphalt in dry and wet conditions (Howson, 2011; Cheng et al., 2002). Aggregate tend to have greater affinity for water when compared to asphalt initiating loss of cohesion or adhesion in the asphalt mix. The adhesive bond energy between asphalt and

aggregate and cohesive energy in asphalt are related to surface free energy of asphalt and aggregate (Cheng et al., 2002). Therefore, the quality of adhesion between asphalt and aggregate is related to the moisture resistance of the asphalt mix (Bhasin and Little, 2007). Developments in physical chemistry in past few decades have enabled to quantify adhesion, if surface energy components of materials involved are known. In the case of an aggregate and binder, proper knowledge of surface energy helps to evaluate the potential of the mix for the chance of moisture damage and thereby useful to find out the right binder- aggregate combination.

Sessile drop device is an emerging technique used for measurement of contact angles on aggregate surfaces and asphalt. In a recent study, Koc (2013) used a sessile drop device for the determination of the surface energy components of different types of aggregates and asphalt and found to be accurate, reliable and economical method. This research makes use of sessile drop method for measuring contact angle on two types of aggregates.

1.2 Objectives of Research

In this study, using sessile drop device contact angles were measured on the surfaces of two aggregates to compute their surface energies.

- Dolese Hartshorne limestone and Mill Creek granite were subjected to polishing using different particle size Silicon Carbide and Aluminium Oxide grits.
- Contact angles were measured on Dolese Hartshorne limestone and Mill Creek granite aggregates at unpolished as well as at different polishing levels.
- Two dimensional and three dimensional roughness parameters were measured in different polishing levels and compared. Surface energy for granite and limestone aggregate were calculated in each polishing level. Energy ratio and compatibility ratio were determined for granite and limestone combined with PG 64-22 neat binder, in each polishing level.

1.2 Organization of the Thesis

Chapter II presents a brief literature review on moisture damage and surface energy. Also, a brief discussion on effect of surface roughness on contact angles and introduction of energy parameters are also included in Chapter II. Chapter III depicts information on need of polishing samples, surface roughness parameters, surface energy calculation and computation of energy parameters. Chapter IV introduces sample preparation whereas Chapter V discusses contact angle measurements on samples and the test protocol followed. Chapter VI presents details on the equipment used for roughness measurements and testing protocol. Chapter VII outlines test results on

- Contact angle measurements on granite and limestone
- Two dimensional and three dimensional surface roughness measurements

Chapter VIII and IX discusses surface energy calculations and determination of energy parameters for granite, limestone and PG 64-22 asphalt binder. Chapter X presents the discussion on test results whereas Chapter XI contains conclusions on test results. Chapter XII illustrates the future suggestions for this research topic.

CHAPTER II

REVIEW OF LITERATURE

2.1 Moisture sensitivity and surface energy

Loss of strength and durability of asphalt mixtures caused by the presence of water is termed as moisture damage (Yilmaz and Sargin, 2012). Moisture damage causes distresses in pavements such as, stripping, bleeding rutting, cracking, raveling etc. As the moisture infuses in the pavement, the moisture damage gets accelerated and the pavement becomes more and more susceptible to moisture (Yilmaz and Sargin, 2012). In literature, there are several theories that explain the mechanism of moisture damage in asphalt, such as detachment, displacement, spontaneous emulsification, film rupture, pore pressure, hydraulic scouring and pH instability (Yilmaz and Sargin, 2012, Howson et al., 2007). Of these mechanisms, detachment and pH instability is explained by interfacial energy theory (Kiggundu and Roberts, 1988). Further, it is believed that the moisture damage occurs due to combination of one or more mechanisms. Bhasin (2006) explained that there are three mechanisms behind the moisture damage of asphalt mixtures and these are (i) mechanical adhesion, (ii) physical adhesion and (iii) chemical bonding. Further, Bhasin (2006) added that the mechanical interlocking and the physical adhesion or the chemical debonding of the asphalt and aggregate system and the chemical reactions at the interfaces of asphalt and aggregate are related to the surface energies of asphalt and aggregate.

Based on surface energy calculations, Cheng et al. (2003) pointed out that affinity of aggregates for water is far greater than the affinity for asphalt. Therefore, when water has access to the

aggregate surface, the asphalt binder might get replaced by water and this rate of replacement will be a function of asphalt- aggregate bond strength (Howson, 2011). The surface properties of

asphalt binder, aggregate and water will decide the thermodynamic energy potential that drives the moisture damage (Howson et. al, 2011). Majidzadra and Brovold (1968) reiterate that the adhesion between asphalt and aggregates is the key factor that determines the moisture sensitivity of an asphalt mixture. The ability of an asphalt mix to resist the attack of moisture or the affinity towards moisture could be estimated by comparing various energy parameters of the asphalt mix such as adhesive bond energy between asphalt and aggregate in dry condition, cohesive bond energy of asphalt and energy potential of water to displace asphalt from aggregate (Howson, 2011). The adhesive bond energy and cohesive bond energy can be calculated knowing the surface energies of asphalt and aggregate. Cheng et al. (2002) determined surface free energy of asphalt using Wilhemy plate method and the surface free energy components of aggregates using Universal Sorption Device. Little and Bhasin (2006) proposed two energy parameters using the adhesion of aggregate with asphalt and cohesion of asphalt which help to evaluate the sensitivity of asphalt mixes towards moisture damage. Detailed information on the assumptions about the energy parameters is given in the background section in Chapter III. Little and Bhasin (2006) conducted a study on several binders and aggregate combinations in order to evaluate the moisture sensitivity and compared the asphalt mixes using the energy parameters. Further, Hefer et al. (2006) also compared various aggregate combinations to predict moisture susceptibility of mixtures and it has been found that the surface energy parameters can be effectively used as a material selection tool to identify moisture sensitive asphalt mixtures. Therefore, it could be inferred that surface energy characteristics of asphalt when compared with surface energy characteristics of aggregate can be used to select most compatible asphalt for a particular aggregate type.

2.2 Surface Energy Concept

Surface energy is a complex phenomenon and it has a significant role in solving various industrial problems, mainly relating molecular interaction at various interfaces. An interface is referred to

as the borderline between two adjacent bulk phases (Aveyard and Haydon, 1973). The characteristics of molecules at the interface (like solid-liquid, solid-gas, liquid-gas or liquid-vapor) could be different from that seen in the bulk phase. This could be due to the asymmetry of force field suffered by the molecules seen the interface, since there is only less intermolecular interaction compared to the molecules at the bulk phase (Ebril, 2006). The molecules at the surface have no force to balance the inward pull from the molecules at the bulk phase. As a result, there will always be an inward attraction perpendicular to surface which will try to reduce the surface of the phase (Ebril, 2006). This excess free energy associated with the molecules at the surface is referred to as excess surface free energy (Aveyard and Haydon, 1973). The property of a liquid drop to assume a spherical shape (minimum surface area at a given volume) is a manifestation of excess surface free energy. Experimental methods for determining surface energy of solids are divided into two categories – mechanical and thermodynamic. Mechanical methods include crack propagation, strain energy release, crushing and fiber stress (Rhee, 1973). Thermodynamic method consists of techniques such contact angle, heat of immersion, heat of solution and interfacial equilibrium angle (Rhee, 1973).

Contact angle technique offers a simple but very suitable method for determining the solid surface energy and liquid surface energy, as well as liquid–solid interface energy. One of the most commonly used methods for determining contact angle is sessile drop technique. This method is based on the contact angle defined by Thomas young in 1805. When a liquid drop rests on a solid surface, the angle formed by the liquid at its point of contact with the solid is called the contact angle (Figure 2.1).

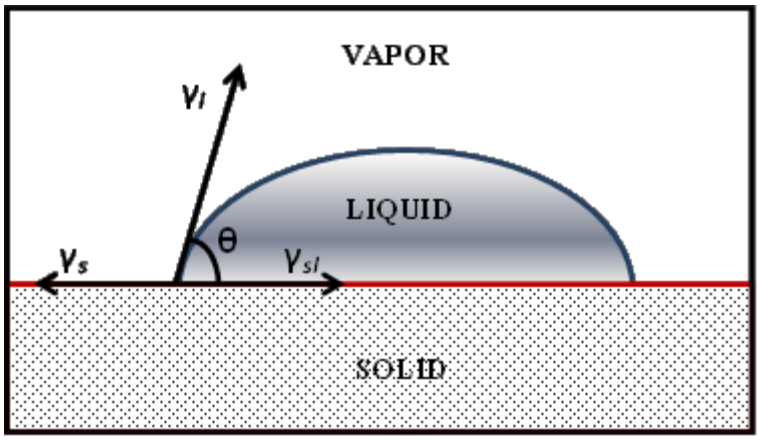

Figure 2.1 Schematic Representation of a Drop Sitting on a Solid Surface Showing the Surface Energy Components.

It can be represented mathematically by the Young's equation (van Oss, 2006).

$$\gamma_l \cos\theta = \gamma_s - \gamma_{sl} \quad (1)$$

Where γ_l, γ_s and γ_{sl} represents the interfacial energies at liquid-air, solid-air, as well as solid-liquid interfaces, respectively, while θ is the contact angle formed between the solid and liquid. The contact angle described by Young is on a plane geometrical solid surface. In practice, it is very difficult to obtain such surface; therefore it is desirable that surface roughness is reduced as much as possible. Therefore, if contact angle are measured on a smooth homogeneous solid surface, it could be useful to predict the surface energy characteristics of the solid material. Recent studies show that surface energy based studies could be used for quantifying the moisture damage potential of asphalt mixes (Cheng et al., 2002; Wasiuddin et al., 2008).

2.3 Equilibrium spreading pressure

In 1937, Bangham and Razouk introduced the condensation of liquid on solid surface would cause complete wetting of solid surface. Authors presented γ_{LV} and γ_{SV} for liquid – vapor and solid

vapor respectively, which was incorporated into Young's equation as shown in Equation 2. Young's equation along with equilibrium spreading pressure is written as

$$\gamma_{sv} = \gamma_{lv} \cos\theta + \gamma_{sl} + \pi_e \quad (2)$$

When solid surface is in equilibrium with liquid vapor, the reduction of surface free energy of the solid due to vapor adsorption is termed as equilibrium spreading pressure, π_e (Lobato, 2004). However, Good (1992) states that for low energy, homogeneous, smooth surface the approximation of π_e are not reasonable. van Oss et al. (1992) also explained that on smooth, homogeneous solid surfaces with finite contact angle the spreading pressure is negligible. Furthermore, Busscher et al. (1986) found that when surface energy of liquid is higher than surface energy of solid, spreading pressures can have considerable effect on contact angle value. However, in the experiments conducted by Busscher et al. (1986) the equilibrium spreading pressures obtained were using alcohol-water mixtures. Fowkes et al. (1980) studied the possibility of spreading pressures associated with high energy liquids deposited on low energy solids, and found that there is no effect of spreading pressure. Fowkes et al.(1980) further explained that when low energy liquid interact with high energy solid and could cause a spreading pressure, which could increase contact angle measured on that surface. Nevertheless, Fowkes (1980) showed that vapor of water (high surface energy liquid) does not spread over low energy polymers. Thin layer wicking experiments conducted by van Oss et al. (1992) showed that there is no effect of spreading pressure on low energy solid surfaces. Therefore, π_e could be neglected in cases where surface energy of liquid is higher than that of surface energy of solid (Yildirim, 2001).

2.4 Contact Angle and Surface Roughness

When a drop is placed on a solid surface, it will maintain a definite area or it will spread on the surface (Cassie, 1948). The spreading of the liquid occurs when energy required to form unit area

of liquid – air interface is less than energy required to form then solid – liquid interface (Cassie, 1948). It is usually considered that a contact angle near to zero represents a hydrophilic surface and a contact angle greater than 90^o represents a hydrophobic surface. However, it is also believed that the surface energy properties of solid material should be considered to determine whether it is hydrophilic or hydrophobic surface. The wettability of a solid surface mainly depends on the surface energy and surface roughness (He et al., 2003). Therefore, the roughness of a solid surface could affect the contact angle measurements. The increased roughness of a surface may modify the interaction of the drop with the solid surface in two different ways. The drop may either reside on the summit of the peaks found on the solid surface incorporating air in between the solid and liquid or it may wet the valleys or grooves. The former case is a composite contact while the latter one is known as the wet contact (Patangar, 2003; He et al., 2004). The concept of apparent contact angle on the composite contact angle is explained by Cassie's equation (Cassie, 1948):

$$\cos\theta_r^c = -1 + \varphi_s(\cos\theta_e + 1) \quad (2)$$

where, θ_r^c is the composite contact angle, φ_s is the fractional contact area of the droplet with the solid surface and θ_e is the equilibrium contact angle on a smooth surface (He et al., 2004; Tavana and Neumann, 2007). Various studies have shown that both the cases are possible on the same rough solid surface (Patankar, 2003; Onda et al., 1996).

Young's contact angle is measured on an ideal solid surface, that is, rigid, flat smooth, chemically homogeneous, insoluble and non-reactive. However, most practical surfaces are rough and therefore it is important to study the surface roughness in order to quantify it. Good (1952) modeled surface geometry as concentric circles to study the effect of roughness on contact angles. Further, Eick et al. (1975) modeled the rough surface as saw tooth surface and developed a theory on contact angle hysteresis. Even though, there were a number of researches on roughness have

been going on for several years, the effects of roughness on sessile drops have not been adequately addressed in the literature. This could be due to the complexity and heterogeneity of the solid surfaces. Bico et al. (2002) explains that roughness makes hydrophilic surface more wettable whereas in the case of a hydrophobic surface, contact angle decreases or it spreads inside irregularities of the solid structure. Further, Bico et al. (2002) points out that when the surface roughness is above 30 μm, there is a chance that the liquid drop will entrap air between the surface irregularities and the liquid drop, which is similar to the idea explained by Cassie (1948).

When a liquid drop encounters a solid surface a droplet formed that consists of a sphere sectioned by the surface. When the liquid is carefully withdrawn from the droplet, the contact angle decreases as the volume of the liquid droplet decreases at a constant contact angle, maintaining the same contact area which is called receding contact angle (Gao and McCarthy, 2006). When liquid is added to a droplet, sitting on a solid surface, the contact angle increases at a constant rate which is called advancing contact angle. The difference between advancing contact angle and receding contact angle is termed as contact angle hysteresis. For ideal solid surfaces, there is no contact angle hysteresis (Kwok and Neumann, 1999). Physical roughness of a surface and chemical heterogeneity are considered as plausible causes for contact angle hysteresis on a surface (Kwok and Neumann, 1999). Kwok and Neumann (1999) suggest that on rough surfaces, contact angles are larger than on chemically identical smooth surfaces. Also, if the surface is rough, there are chances that contact angle will reflect the surface topography rather than surface energy characteristics (Kwok and Neumann, 1999). Kwok et al. (1997) state that if hysteresis is due to surface roughness, the contact angle obtained from a test are meaningless since they do not satisfy the basic assumptions of Young's equation. Therefore it is important that the surface of measurement should not have effect of roughness on contact angle. Hence, it is important to reduce the surface roughness as much as possible so that representative contact angle of the surface is obtained. Also, Kwok et al. (1997) observed that irregular and inconsistent contact

angles are an indication of rough surface. Further, Kwok et al. (1997) state that advancing contact angle on a chemically heterogeneous surface could be a good approximation of Young's contact angle, provided there is no effect of surface roughness. Moreover, Kwok and Neumann (1999) suggest that receding contact angles are not always reproducible due to the sorption of the liquid on to the solid. Furthermore, Cassie (1948) summarizes that advancing contact angles have a unique value whereas receding contact angles do not show a unique value. Giese and van Oss (2002) suggest that retreating liquids cause residual wetting leading to positive contact angle hysteresis. Thus only advancing angles are meaningful when Young Dupre equation is used for calculating surface energy components, because they do not produce residual wetting (Giese and van Oss, 2002). Therefore, for the calculation of surface energy components in this study advancing contact angles are used.

CHAPTER III

BACKGROUND

3.1 Polishing

Effect of surface roughness on contact angles have been studied for decades. Wenzel (1949) was one of the first to discuss the effect of roughness on contact angles. Wenzel proposed a theory in which the increase in the surface area of a roughened plane is shown to be responsible for the change of the contact angle. In order to study the extent of roughness on contact angles it is important to observe contact angles on different levels of roughness. In a study conducted by Tamai and Aratani (1972), advancing contact angles on silica glass with different levels of roughness were measured and found that contact angles were affected by roughness of the surface and Wenzel's theory was verified. Further, in a study using polymers, Busscher et al. (1984) observed that the influence of roughness on contact angles significantly reduced when the surface roughness R_a falls below 0.1 micro meters. For the study, Busscher et al. (1984) used carborundum paper, diamond pastes and Aluminium oxide powders of different particle sizes for polishing the samples. Different particle size Silicon Carbide grits were employed by Yavuz et al. (2011) in order to reduce surface roughness of different building tiles. Furthermore, Ceyanoglu and Gorgulu (2008) used several silicon carbide grits in order to reduce surface roughness on limestone and marble samples. Since the contact angles represent the surface energy characteristics of the solid material, it is important that surface roughness is reduced as much as possible. Therefore, in this research, the abrasives selected to polish the samples were 400, 600 and 100 grade Silicon carbide grits and 5 micron and 3 micron Aluminium Oxides.

3.2 Surface Roughness

Accurate measurement of contact angle is important since the surface energy components are related to it (Zhou and Hosson, 1995). Therefore, it is important to quantify surface roughness and reduce the surface roughness as much as possible for obtaining representative contact angles for the corresponding surfaces. Following are some important roughness parameters which are used to quantify surface roughness generally:

(i) Arithmetic mean roughness (R_a) - R_a is defined as the average absolute deviation of surface irregularities from a mean line along the assessment length of the profile:

$$R_a = \frac{1}{l}\sum_{i=1}^{n} y_i \quad (3)$$

where, y is the height of the peak/valley from the mean line and n is the number of measurements along the measurement length l as shown in Figure 3.1. This parameter gives a general description of roughness of the sample surface (Gadelmawla et al., 2002).

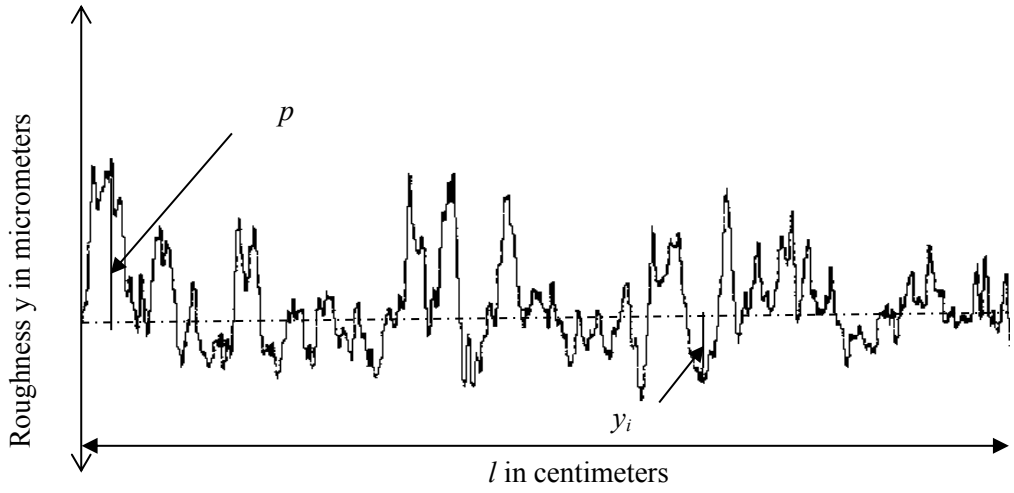

Figure 3.1 Roughness Profile of a Surface Showing the Assessment Length.

(ii) Ten point height (R_z) – R_z is defined as the difference in height between average of the five highest peaks and the five lowest valleys along the assessment length of the profile. In Figure 3.1, *p* represents the highest peak in the assessment length *l*.

(iii) Root mean square roughness (R_q) - R_q is also known as RMS. It represents the standard deviation of the distribution of surface heights. This is an important parameter when describing surface roughness by statistical methods. This parameter is more sensitive than R_a.

(iv) Maximum height of the peaks (R_p) - R_p is defined as the maximum height of the profile above the mean line within the assessment length.

(v) Maximum depth of the valleys (R_v) – Rv is defines as the depth of the profile below the mean line within the assessment length.

(vi) Maximum height of the profile (R_t or R_{max}) - R_t or R_{max} is defined as the vertical distance between the highest peak and lowest valley along the assessment length of the profile. This parameter is very sensitive to high peaks or deep scratches.

(vii) Skewness (R_{sk}) – Skewness of a profile is the third central moment of profile amplitude probability density function, measured over the assessment length. This parameter is used to measure the symmetry of the profile about the mean line. Also, this parameter is sensitive to occasional deep valleys or high peaks.

(viii) Kurtosis (R_{ku}) – Kurtosis coefficient is the fourth central moment of the profile amplitude probability density function, measured over the assessment length. This parameter describes the sharpness of the probability density of the profile.

3.3 Surface Energy components

Direct measurement of surface energy of solids is hardly achievable. However, it is feasible to measure different interactions between solids and liquids due to surface energies of solid liquids and gases. One fine example of such interactions is the contact angle defined by Thomas Young.

Young explained interfacial interactions on a solid surface with a liquid drop using the Equation 1 (as explained in Chapter II), has undergone several modifications. Good Van Oss Chaudhury method (GVOC) is one of the popular methods for calculating surface energies of materials using contact angles. In Equation 1, γ_l and cos θ are the known and γ_s and γ_{sl} are unknown parameters. However, the combination of Dupre equation (Equation 2 given below) and Equation 1 can be used along with three probe liquids (i.e., water, Diiodomethane(DIM), ethylene glycol (EG)) to determine contact angles on the surfaces of solid materials. Dupre equation represents the free energy of interaction between a solid and a liquid:

$$\Delta G_{sl} = \gamma_{sl} - \gamma_s - \gamma_l \quad (3)$$

where, ΔG_{sl} represents the free energy of interaction between the solid and the liquid. Combining Equation 1 and Equation 3 results in the Young-Dupre equation (4):

$$(1 + cos\theta)\gamma_l = -\Delta G_{sl} \quad (4)$$

Surface energy of natural substances can be divided into polar and non-polar components (Miller et al., 2012).Dipole-dipole interactions and induced dipole interactions cause non-polar, van der Waals or dispersive components (van Oss, 2006). Electron donor or electron acceptor interactions will produce polar or non-dispersive interactions. Polar interactions are further divided into electron donor (Lewis acid) and electron acceptor (Lewis base) components (van Oss et al., 1988). The total interaction energy consists of Lifshitz-van der Waals and Lewis acid-base interaction components:

$$\Delta G_{sl} = \Delta G_{sl}^{LW} + \Delta G_{sl}^{AB} \quad (5)$$

In terms of individual surface energy components, Equation 5 takes the form:

$$\Delta G_{sl} = -2\left(\sqrt{\gamma_s^{LW}\gamma_l^{LW}} + \sqrt{\gamma_s^{+}\gamma_l^{-}} + \sqrt{\gamma_s^{-}\gamma_l^{+}}\right) \quad (6)$$

where, γ_l^{LW} is the Lifshitz-van der Waals component of liquid; γ_s^{LW} is the Lifshitz-van der Waals component of solid; γ_l^{+} is the Lewis acid component of liquid; γ_s^{+} is the Lewis acid component of solid; γ_l^{-} is the Lewis base component of liquid; and γ_s^{-} is the Lewis base component of solid. The

combination of Equation 4 and Equation 5 gives the complete Young-Dupre equation that is widely used in determining the surface energy components of solid materials using contact angle measurements (van Oss, 2002):

$$(1 + cos\theta)\gamma_l = 2\left[\sqrt{\gamma_s^{LW}\gamma_l^{LW}} + \sqrt{\gamma_s^{+}\gamma_l^{-}} + \sqrt{\gamma_s^{-}\gamma_l^{+}}\right] \quad (7)$$

Equation 6 is generally known as the Good-van Oss-Chaudhury (GVOC) or acid-base approach.

3.4 Energy Ratio and Compatibility Ratio

Based on the surface energies of asphalt binders and aggregate, three quantities that influence the moisture sensitivity are:

- Work of cohesion in asphalt binder
- Work of adhesion between asphalt and aggregate
- Work of debonding or reduction of free energy when asphalt is replaced by water

Therefore, in order to quantify the moisture sensitivity of the asphalt mixtures, it is important to determine the adhesion of the asphalt with aggregate, cohesion of the asphalt and the adhesion of asphalt and aggregate when the moisture is present. Gibbs free energy of cohesion or work of cohesion is defined as the work to be done to separate a column of a liquid with unit cross sectional area into two. The Gibbs free energy of cohesion or the work of cohesion is given by (van Oss, 2002):

$$\Delta G_i^c = -2(\gamma_i^{LW} + 2\sqrt{\gamma_i^{+}\gamma_i^{-}}) \quad (8)$$

where i denotes the asphalt in the asphalt-aggregate mixture. In fracture mechanics, work of cohesion of asphalt binders is a significant parameter to determine energy required for the growth of micro cracks within the asphalt binder phase of mastic of asphalt mixture. The amount of work required to separate two different materials at their interface in vacuum is known as the work of adhesion or the Gibbs free energy of adhesion. Based on the acid-base theory, the work of adhesion of two materials can be expressed as the function of the surface energy components as follows (van Oss, 2002; Little and Bhasin, 2006):

$$\Delta G_{ij}^{a} = -2\sqrt{\gamma_i^{LW}\gamma_j^{LW}} - 2\left(\sqrt{\gamma_i^{+}\gamma_j^{-}} + \sqrt{\gamma_i^{-}\gamma_j^{+}}\right) \quad (9)$$

This energy is also known as dry adhesion energy. The more the dry adhesion energy between the binder and aggregate, the more will be their resistance to external moisture energy. Adhesion and cohesion energies in the asphalt mixture are altered when moisture enters the system. Moisture causes damage to asphalt mixture and affects longevity of pavement. The free energy of adhesion when moisture is present in the asphalt mixture is given as Equation 7:

$$\Delta G_{ikj}^{a} = 2\left[\begin{array}{c}\sqrt{\gamma_i^{LW}\gamma_k^{LW}} + \sqrt{\gamma_j^{LW}\gamma_k^{LW}} - \sqrt{\gamma_i^{LW}\gamma_j^{LW}} - \gamma_k^{LW} + \\ \sqrt{\gamma_k^{+}}\left(\sqrt{\gamma_i^{-}} + \sqrt{\gamma_j^{-}} - \sqrt{\gamma_k^{-}}\right) + \sqrt{\gamma_k^{-}}\left(\sqrt{\gamma_i^{+}} + \sqrt{\gamma_j^{+}} - \sqrt{\gamma_k^{+}}\right) \\ -\sqrt{\gamma_i^{+}\gamma_j^{-}} - \sqrt{\gamma_i^{-}\gamma_j^{+}}\end{array}\right] \quad (10)$$

Little and Bhasin (2006) stated that the displacement of asphalt by water in asphalt aggregate system is a thermodynamically favored phenomenon. In their research study, all aggregate binder systems which are analyzed showed that total work done on the system during the displacement process is less than zero. Majidzadra and Brovold (1968) also reinstates that the water-aggregate interface reduces the free energy of aggregate interface more than aggregate –asphalt interface, thus making it a thermodynamically favorable activity. Using Equation 9 and Equation 10, Little and Bhasin (2006) introduced a parameter known as the compatibility ratio (CR):

$$CR = \left|\frac{\Delta G_{ij}^{a}}{\Delta G_{ikj}^{a}}\right| \quad (11)$$

The CR was derived on the assumption that the adhesion between the asphalt binder and aggregate is directly proportional to the moisture resistance and inversely proportional to the work of debonding (Little and Bhasin, 2006). CR simply compares the work adhesion in dry condition to the work of adhesion in wet condition. However, CR parameter does not take wettability of asphalt binder into account. Wettability is the ability of a material to wet another

material. Wettability also determines the ability of a material to impregnate into the micro textural features of solid surface. Given the aggregate surface, the asphalt binder with better wettability has strong affinity to coat the aggregate surface than an asphalt with lower wettability. Also, better coating of aggregates will help to reduce the weak points in asphalt aggregate mixture. It is the cohesive bond energy of asphalt which determines the wettability of the aggregate in the mix (Bhasin, 2006). Considering the cohesive bond energy of the asphalt binder, another parameter, energy ratio (ER) was introduced (Little and Bhasin, 2006; Howson, 2011):

$$\mathrm{ER} = \left| \frac{\Delta G_{ij}^{a} - \Delta G_{i}^{c}}{\Delta G_{ikj}^{a}} \right| \tag{12}$$

In this study, the sensitivity of Equation 11 and Equation 12 were evaluated for various levels of roughness of two different aggregates (i.e., Mill Creek granite and Dolese Hartshorne limestone) and one asphalt binder (i.e., PG 64-22). The combination of asphalt binders and aggregates with highest magnitude of energy parameters (ER and CR) will be relatively more resistant to moisture damage than other combinations.

CHAPTER IV

MATERIALS AND SPECIMEN PREPARATION

4.1 Samples

For the experiments in this study two samples of limestone and granite are selected. Limestone is obtained from Dolese Hartshorne quarry which is located approximately 1.2 miles south of Hartshorne, Oklahoma. The quarry is extracting limestone from the Pennsylvanian Wapanucka Limestone. The Wapanucka Limestone is approximately 314 million years old, and formed in a shallow, high energy environment.

Mill Creek Granite comes from the Martin Marietta Materials quarry located approximately 3.4 miles south of Mill Creek Oklahoma. The quarry is located on the Tishomingo Granite, a Proterozoic (1.374 billion years old) granite composed primarily of pink feldspar (microcline), quartz and biotite.

4.2 Specimen preparation

Large size rocks of Dolese Hartshorne limestone and Mill Creek granite obtained were about 10-20 cm of diameter. These were sliced to 1-2 cm thickness and 2.5 cm x 3.5 cm cross sectional area approximately, for the convenience of handling and polishing. Hill Quist RF 20-24 slab saw (Figure 4.1) was used for slicing the large rocks. The samples obtained after cutting were washed with soap and water in order to remove the oil and any other particle residue resulted from cutting.

Further, these samples were rubbed with hexane saturated paper towels in order to remove the oil completely. Following that, the samples were washed thoroughly with soap and water. Samples are dried in the oven at 105 ± 5^{o} C for 12 hours and then kept in the desiccator for another 12 hours. After the samples cooled down to room temperature in the desiccator, contact angle are measured using sessile drop device. Calcium sulfate crystals were kept in desiccator in order to keep the samples moisture free. Before taking the roughness measurements, the same protocol of cleaning and drying are followed.

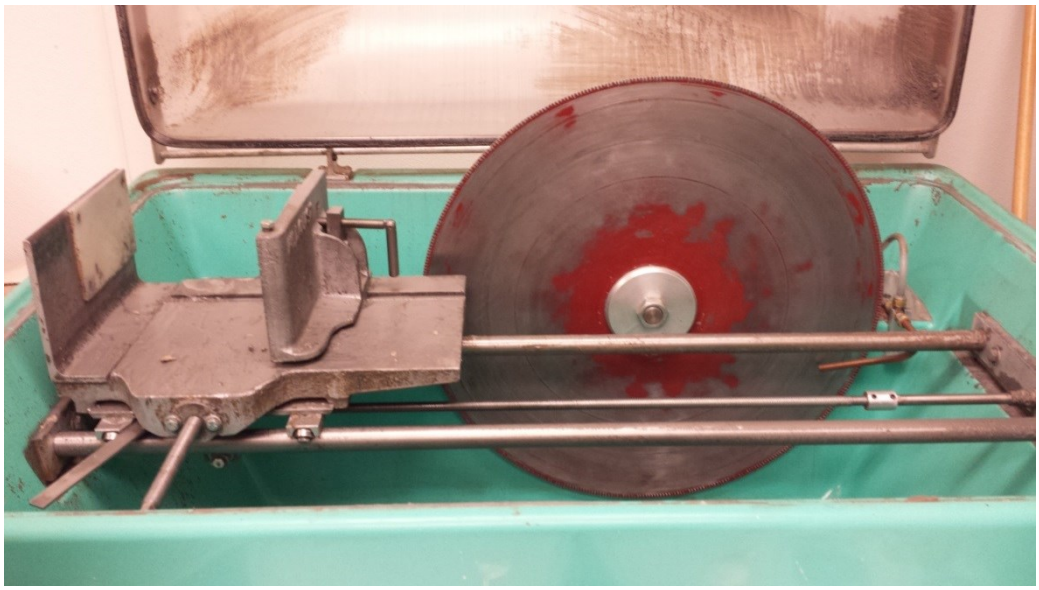

Figure 4.1 Hill Quist RF 20-24 Slab Saw used for Cutting the Rocks.

Even though the diamond saw cut the rocks relatively smooth, there were traces of the blades. However, before polishing the samples, contact angles and roughness were measured. Following that, the samples were polished with Silicon Carbide 400 grit (400 SiC). The polishing process was carried out on a grinding wheel by manually holding the sample on the rotating plate for 20 minutes. Care was taken to apply uniform pressure on the sample so that sample was polished uniformly. After polishing the samples, washing, drying and desiccation process was completed before conducting contact angle and roughness measurements. After each set of

contact angle measurements samples were washed and dried as explained earlier. Further, samples were subjected to a series of polishing by Silicon Carbide 600 (SiC-600), and Silicon Carbide 1000 (SiC-1000), followed by Aluminum Oxide 5 micron (Al_2O_3-5μ) and Aluminum Oxide 3 micron (Al_2O_3-3μ) grits. Of these, 600 SiC polishing was performed on the same grinding wheel as mentioned earlier.

Polishing with finer grits such as 1000 SiC (particle size 9.2 μm), Al_2O_3-5μ and Al_2O_3-3μ were performed manually on a glass plate by making a paste of respective grit. On the glass plate, a thick paste of abrasive grit was made with distilled water. Polishing is performed by holding down the sample on the glass plate and moving in a circular motion for 20 minutes. The polishing set up on glass plate is shown in Figure 4.2. Washing and drying processes, contact angle measurements and roughness measurements were repeated after each polishing.

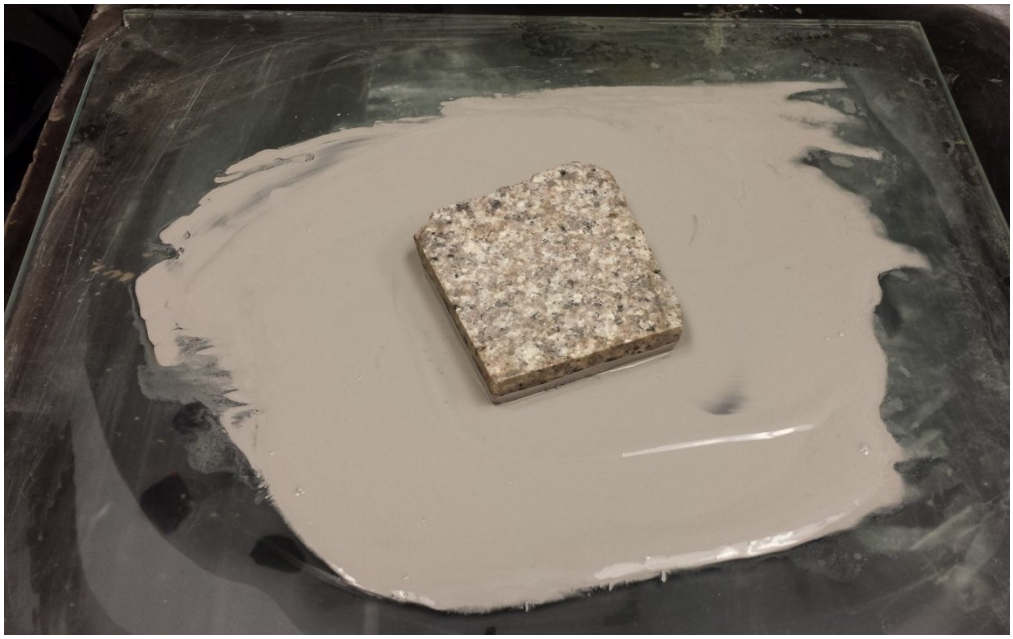

Figure 4.2 Polishing of Samples Using Glass Plate and Abrasive Paste.

Five points were identified on the sample and contact angle measurements were performed on these points at all the polishing stages. Figure 4.3 shows selected points on granite and limestone

for contact angle and roughness measurements. Contact angle measurements were conducted on 1, 2, 3 4 and 5 points for both samples. Five repetitions were made on each of the five points and average is taken for the all the repetitions to find the overall contact angle.

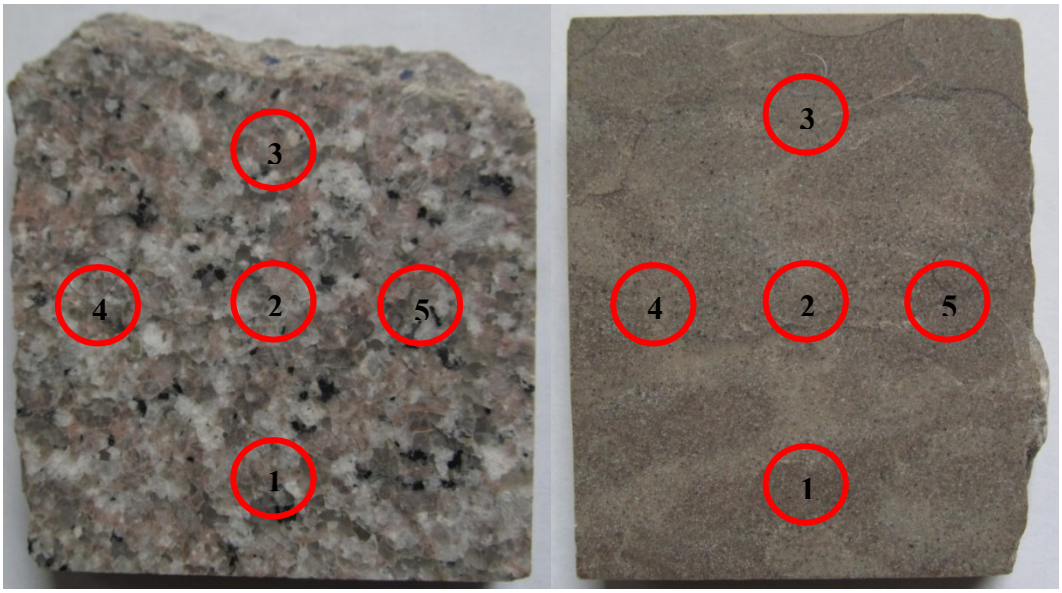

Figure 4.3 Mill Creek Granite and Dolese Hartshorne Limestone Rock Samples Used in the Study.

However, the two dimensional roughness measurements were conducted on 1, 2, 4 and 5 points for both samples. For the non- contact optical profilometer, two points for each samples were chosen (1 and 5). An area of 1 cm x 1 cm was scanned and roughness parameters were calculated from the scanned area for each of the selected points.

CHAPTER V

CONTACT ANGLE MEASUREMENTS

5.1 Sessile Drop Device

Sessile drop method offers quite simple, yet useful method for measuring contact angles on aggregates and asphalt. This device makes direct measurement of contact angle of a drop which is placed on a prepared flat surface by acquiring the image of the drop.

FTA 1000 B series sessile drop device is used in this research experiment for measuring contact angles. The device has a camera equipped with a microscopic lens for obtaining images of sample. The magnification and focus of camera is mechanically adjusted to obtain the correct perspective of the liquid drop. This is achieved by moving the lens forward and backward by two rear mounting screws. A stepper motor driven automatic syringe is equipped with the instrument by which probe liquid drops are dispensed on to the specimen surfaces. Schematic drawing of sessile drop device is shown in Figure 5.1.

Probe liquids can be dropped to the surface of the samples or they can be touched off by raising the platform or specimen stage provided. In this study, the probes liquids are made to touch off the sample surface. Samples are kept on a platform (or specimen stage) by which samples can be moved forward backward and upward according to the selected position of measurement by adjusting screws. The height of the platform is adjusted so that the pendant drop is touched off by the surface of the flat specimen.

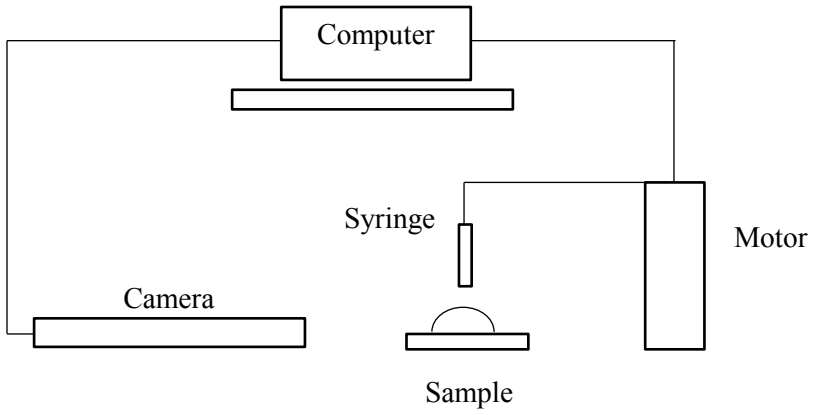

Figure 5.1 Schematic drawing of a sessile drop device showing major components.

Different diameters of syringes are selected according to the viscosity of the probe liquid used. In this research, Hamilton gas tight syringes are used for taking probe liquids.

Ethylene glycol (EG), diiodomethane (DIM) and distilled water are the probe liquids used for the contact angle measurements. The surface tension of probe liquids is as given in Table 5.1.

Table 5.1 Surface Energy Components of Probe Liquids Used in This Study (Giese and van Oss, 2002).

Liquid Probe	γ^{Total}	γ^{LW}	γ^{AB}	γ^{-}	γ^{+}
	(ergs/cm^2 or mJ/m^2)				
Water	72.80	21.80	51.00	25.50	25.50
Diiodomethane	50.80	50.80	0.00	0.00	0.00
Ethylene Glycol	48.00	29.00	19.00	1.92	47.00

γ^{Total} = Total surface energy of probe liquid

γ^{LW} = Lifshitz van der Waal's surface energy component

γ^{AB} = Total acid base component of surface energy

γ^- = Base component of surface energy

γ^+ = Acid component of surface energy

The syringe pump can push out or pull in the fluid. The instrument can also be equipped with a manual syringe, if needed. Also, the instrument has a tilting stage which can be tilted up to 90^o. Both of these features can be utilized to measure advancing as well as receding contact angles. Figure 5.2 shows the basic set up of sessile drop device.

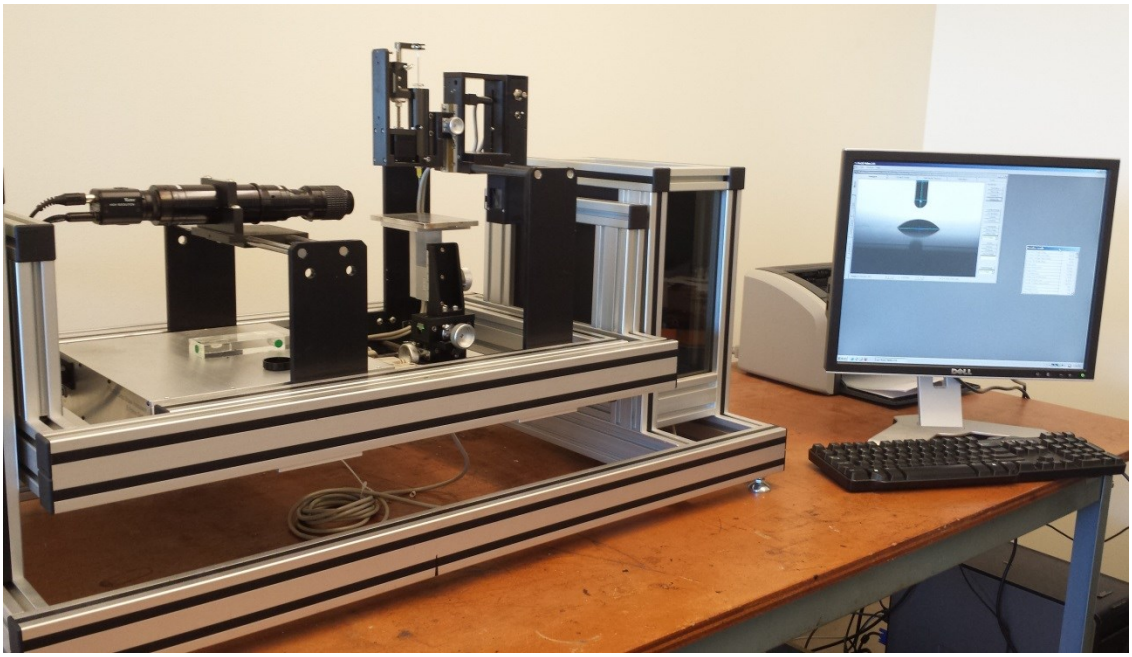

Figure 5.2 Sessile Drop Device

The liquid probe drop is analyzed by the software for contact angles, interfacial tension, pendant and sessile drop volumes, and spreading. Before conducting any measurements on samples, the magnification of the instrument is calibrated using a standard ruby hemisphere. The procedure of calibration is as explained in Section 5.2.1.

5.2 Test protocol

5.2.1 Calibration of Sessile Drop Device

A standard ruby hemisphere of 90 ± 1 ^{o} is used for calibrating the sessile drop device. The ruby hemisphere is first placed on the platform. A series of images are taken and average contact angle is observed and checked with the calibration standard. If the average angle did not read with in the allowable limit, the magnification of the lens is adjusted. The whole process of taking photograph and checking with calibration standard is repeated until the average contact angle reads within 90 ±1^{o} . Figure 5.2 shows the photograph of ruby hemisphere during the calibration process.

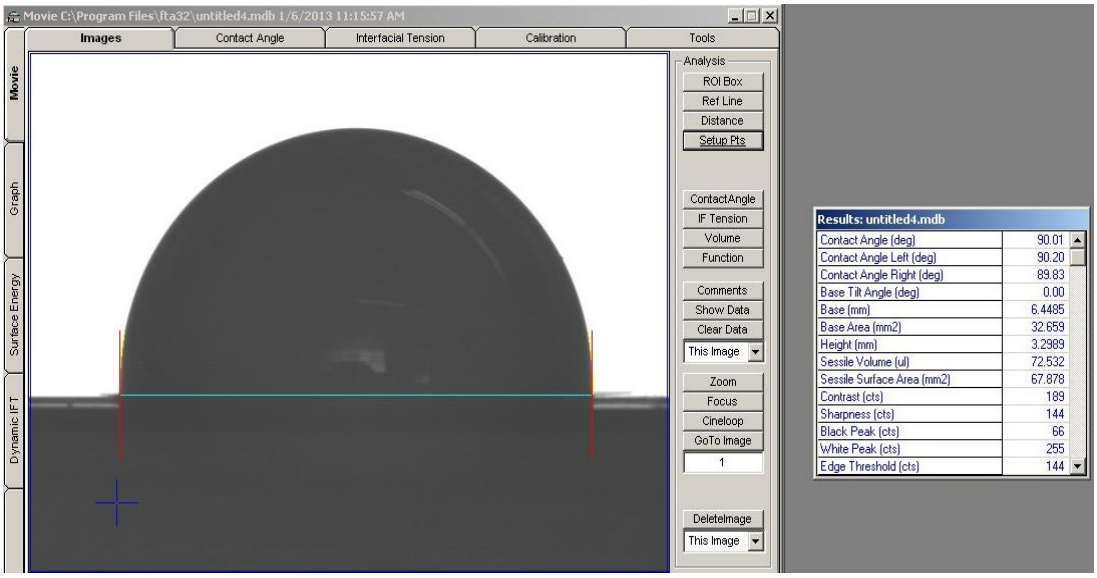

Figure 5.3 Photograph of Ruby Hemisphere Used for The Calibration of The Sessile Drop Device.

5.2.2 Measurement of Contact Angles

Samples were cleaned as explained in Chapter IV and were kept on the platform of the instrument. One 500 microliter and two 100 microliter Hamilton gas tight syringes are used for filling and dispensing distilled water, ethylene glycol and diiodomethane, respectively. Fully

automated syringe is used to dispense the probe liquids. For all of the probe liquids, volume of drops used was ten to twelve microliter. The pump is started and the drop is allowed to form, when the drop is in its full pendant form, the specimen stage is raised and the drop is allowed to touch off the sample. As soon as the drop was deposited on the sample surface images were captured by the camera and are analyzed using a data analysis software. As the probe liquid drop is placed on the aggregate surface, it spreads over the sample surface over a few seconds until the force equilibrium is established between the surface energies of the probe liquid and aggregate surface. The images of the changes of contact angles the liquid drop makes on the aggregate surface are captured from the point where the drop is placed on the surface for over a period less than one minute, during which approximately 60 images are recorded. After the drop is deposited on the sample, the software fits a mathematical expression and estimates an average contact angle by determining the slopes of the tangents to the drop at the point where it is in contact with the aggregate surface. Figure 5.3 depicts a screenshot of the FTA software showing the liquid drop sitting on the aggregate surface.

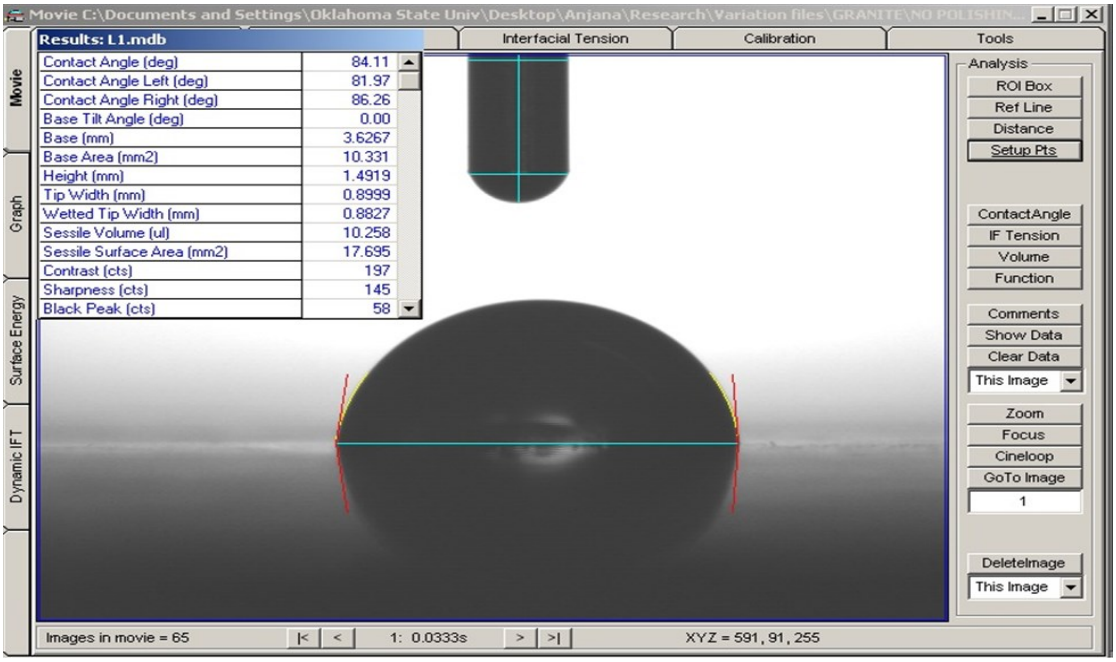

Figure 5.4 Photograph Showing Drop Sitting on Sample Surface.

The output obtained after the analysis contains average contact angle over a time period with in one minute (around 60 images). The software is enabled to adjust the number of images per second as well as the duration of the test. Time period for single test was 60 seconds for this study. As shown in Figure 5.3 a number of parameters such as right and left contact angles, base area of drop, sessile volume, sessile surface area etc. other than the average contact angle were obtained in the output window. A plot between time elapsed and contact angle can also be seen in the output window (Screen shot of the plot is given in Appendix A).

CHAPTER VI

ROUGHNESS MEASUREMENTS

In order to reduce effect of roughness on contact angles, the samples are subjected to series of polishing stages. Also, it is important to quantify the surface roughness of the sample undergoing polishing to interpret the results. At each polishing, surface roughness of the samples were measured. Further, the roughness measurements were performed using two methods such as two dimensional and three dimensional profilometers. This Chapter outlines the two methods of surface roughness measurements.

6.1 Two dimensional Roughness measurements

A stylus type profilometer (Mahr Perthometer) is used for 2D measurement of surface roughness. Figure 6.1 shows the schematic diagram of profilometer (Mahr Perthometer) used in this study.

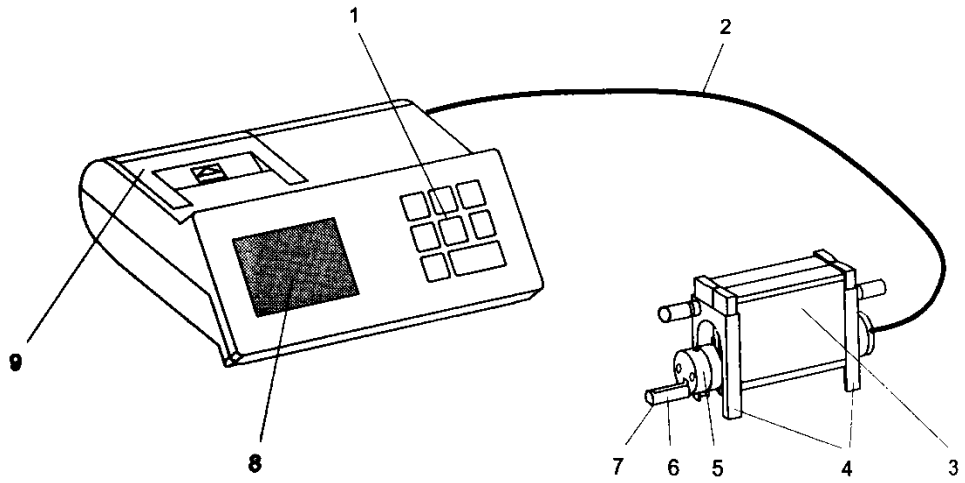

Figure 6.1 Schematic drawing of Mahr perthometer.

The equipment parts shown in Figure 6.1 are defined as:

1- Keypad
2- Connecting cable
3- Hand held support
4- Vertical adjusters
5- Dive unit PFM
6- Vee pick up protection
7- Pick up (stylus)
8- Display
9- Printer cover

Profilometer consists of a drive unit on which the pick-up is connected. Pick up is that part of the profilometer with stylus which is connected to the drive unit. Drive unit moves at constant speed in a straight line during a measuring run across the surface to be tested. For the experiments in this study, pick-up travels in longitudinal direction to make measurements on the sample surface. The pick-up is equipped to travel in lateral as well as upward to make measurements. Vertical adjusters are employed to connect with the hand held support so that height of the pick is adjusted. Vee pick up protection provides necessary protection for the pick up. The tracing length for this study was 5.6 millimeter. Figure 6.2 shows the photograph of the profilometer set up for measuring limestone sample. The output of the profilometer gives the roughness parameters R_a , R_z and R_{max} . These parameters are explained in Chapter III.

The sample surface is cleaned and the profilometer set up is switched on. The stylus of the profilometer is adjusted to the height of measurement according to the sample. The pick up travels in longitudinal direction to measure the roughness parameters. Roughness is measured on four locations as shown in Figure 4.3. Avergae of the four measurements is taken as the avergae R_a for the sample for the particular polishing stage.

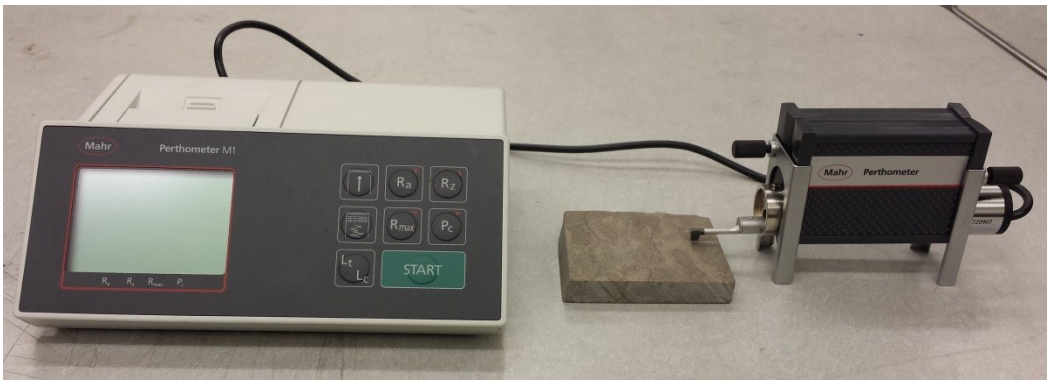

Figure 6.2 Perthometer set up for measuring limestone aggregate sample.

6.2 Three dimensional (3D) profilometer

Nanovea PS50 optical profilometer is used for measuring the 3D roughness. The system consists of a base and CHR. CHR is axial chromatism optical sensor used for measuring height information of the surface. The axial chromatism technique uses a white light source, where a light passes through an objective lens with high chromatic aberration. When the measured sample is within the range of possible heights of the instrument, the incident white light is focused to form the image of the surface. Only focused wavelength is allowed to pass through the spatial filter and spectral analysis is done using diffraction grating. Figure 6.4 shows the photograph of Nanovea profilometer connect to a computer.

Optical pen is designed to determine vertical measurement range and optical resolutions. Data acquiring software, Nanovea 3D is used to operate the profilometer. When compared to 2D profilometer, a number of roughness parameters are obtained from optical profilometer. The area to be measured is specified by entering the dimensions of area in the software window. Also, the rate of acquisition of the data is specified along with the area. Appendix A shows the picture of the input window of nanovea 3D software. Basic components in the 3D profilometer set up is given in Figure 6.3.

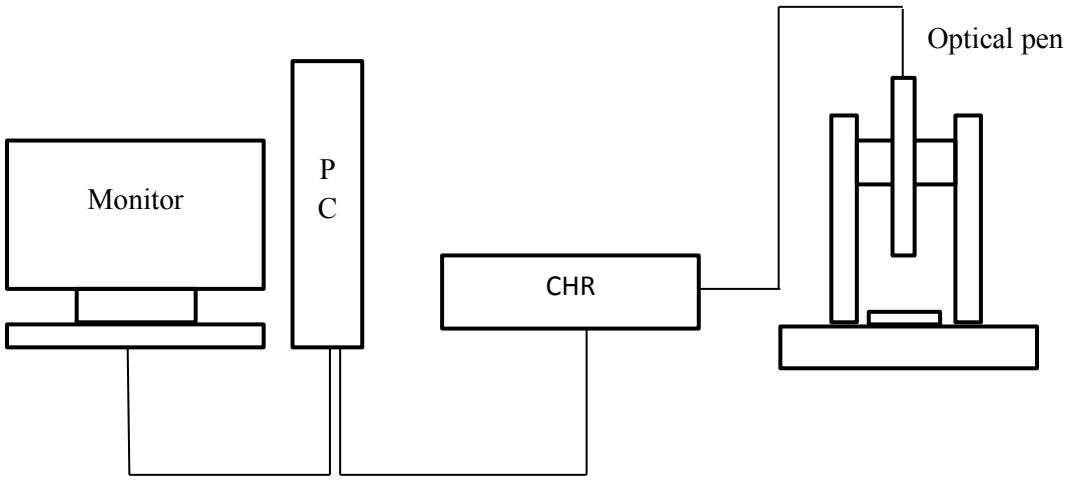

Figure 6.3 Major Components of 3D Optical Profilometer Set up.

Pattern of surface topography of the sample can also be obtained along with the output. The sample with cleaned surface is kept on the stage below the optical pen. Typical output from Nanovea profilometer is attached in Appendix A. The speed of acquisition used in this study is 20 steps. The size of the area selected on sample was 1 cm x 1 cm. Two points on each sample were measured using 3D profilometer. Ten Ra values were measured from one 1 cm x 1 cm area and average is calculated.

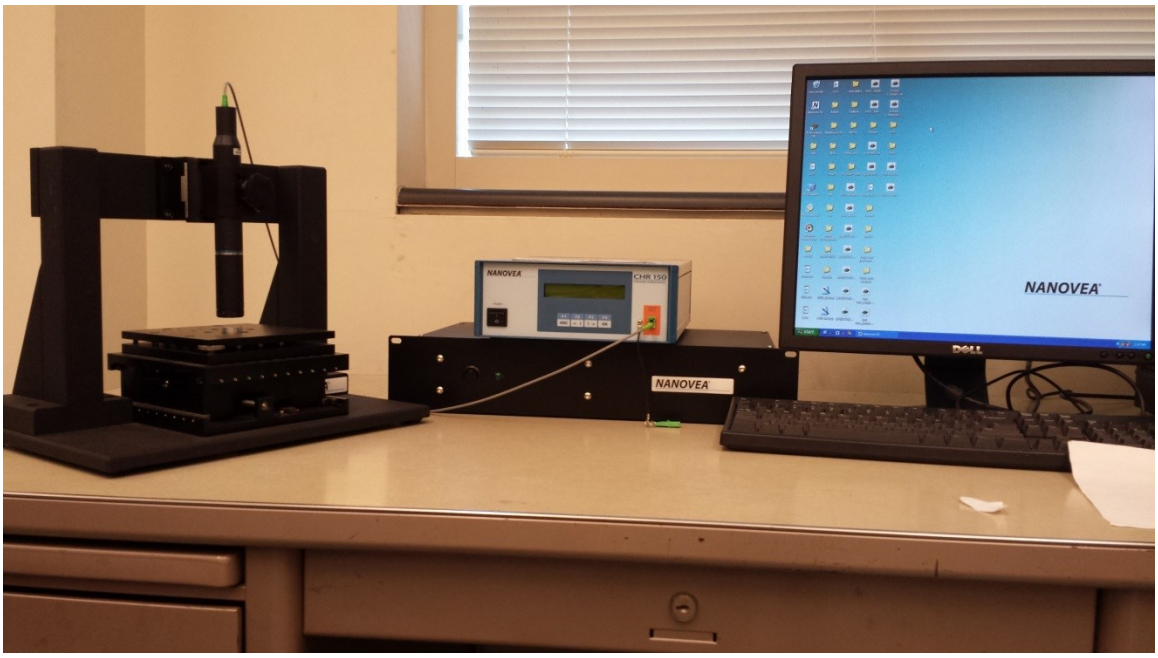

Figure 6.4 Nanovea Optical Profilometer.

CHAPTER VII

TEST RESULTS

7.1 Contact Angles

Contact angles were measured on Dolese Hartshorne limestone and Mill Creek granite using sessile drop device. On the unpolished sample as well as after each polishing stage, contact angle measurements were conducted on previously identified five locations (as shown in Figure 4.3). Water, ethylene glycol (EG) and diiodomethane (DIM) were used as the probe liquids for measuring contact angles. Five repetitions were made on each five locations and average of all the repetitions are considered as average contact angle for the sample at that particular polishing stage. The average contact angles for all the three liquids at each polishing stage for granite and limestone are plotted to evaluate the variation.

7.1.1 Dolese Hartshorne Limestone

Results show that contact angles with all the probe liquids on limestone exhibited a decreasing pattern as the polishing progressed. Figure 7.1 shows the variation of contact angles with water, ethylene glycol and diiodomethane in different polishing stages. In Figure 7.1, error bars show the standard deviations of contact angle in the corresponding polishing stage. Water displayed highest contact angle in all the polishing stages than other two probe liquids. From the rough sample to polishing with 600 SiC grit, the contact angle of water did not change considerably. However, there was significant variation in the standard deviation. Standard deviation of water

has decreased from 5.17^{o} to 1.8 ^{o}. Though, when all the polishing stages were finished, the standard deviation of contact angles obtained with water was 1.67 ^{o}. Data used for calculation for average contact angle at each polishing stage is attached in the Appendix B.

EG indicated an increase in standard deviation in the 600 SiC polishing stage. This could be attributed to the calibration techniques introduced after the 600 SiC polishing. Also, further polishing stages after the calibration technique was introduced, the standard deviation decreased, showing that the contact angles on the sample surfaces become consistent.

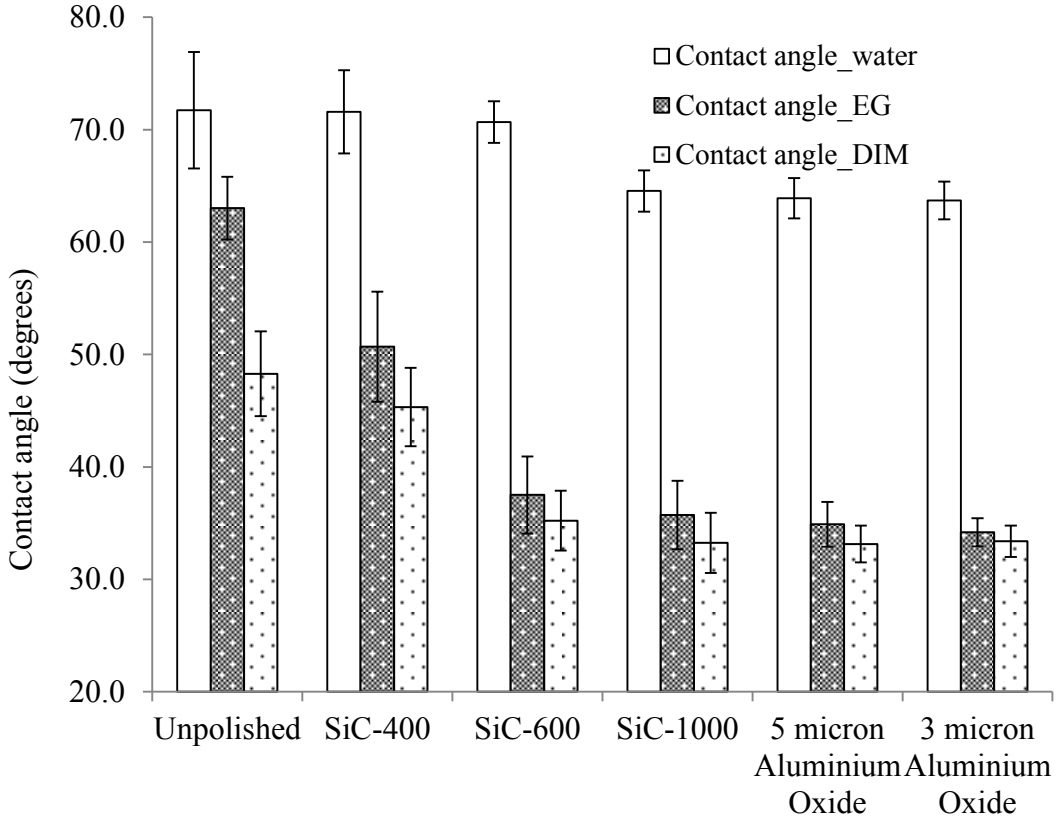

Figure 7.1 Variations of Contact Angles of Water, Ethylene Glycol and Diiodomethane in Different Polishing Stages.

7.1.2 Mill Creek Granite

On granite sample, contact angles with all of three probe liquids showed decreasing pattern, as similar to the contact angle variation in limestone. Figure 7.2 shows the variation of contact angle with water, EG and DIM in all the different polishing stages. Unlike in the case of limestone, the change of contact angle with water after the initial polishing stage was significant for granite. Standard deviation of contact angles with water varied considerably in the initial polishing stages. On the rough sample water contact angles showed a standard deviation of 3.74^{o}, which changed to 4.8^{o} when polished with 400 SiC. However, further polishing produced lower contact angles up to the final polishing with 3 micron Aluminium Oxide with a standard deviation of 1.22^{o}. Contact angles with ethylene glycol displayed pattern of the variation similar to that of contact angle with water. Even though the contact angles decreased, the standard deviations of ethylene glycol increased after the first polishing level. As explained in the previous section, introduction of calibration techniques might be the reason of change in standard deviation. Calibration technique helped to standardize the measurement of contact angles on the samples in all the polishing stages followed after 400 SiC.

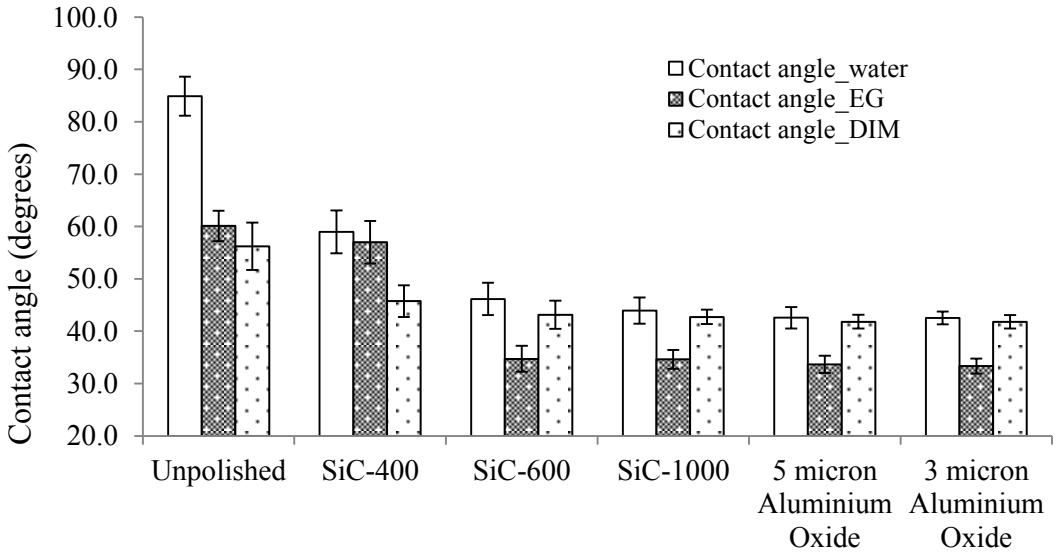

Figure 7.2 Variations of Contact Angles of Water, Ethylene Glycol and Diiodomethane in Different Polishing Stages.

7.2 Surface Roughness

In the present study, two methods of determining surafce roughness is employed to quantify the surface roughness of samples. Surface roughness of Dolese Hartshorne limestone and Mill Creek granite were measured right after cutting with diamond saw as well as after each stage of polishing. Roughness was measured using contact and non-contact profilometers and the results were plotted against different polishing stages.

7.2.1 Two dimensional method of surface roughness measurement (Contact Method)

Surface roughness was measured using Mahr perthometer, on the loctions numbered 1, 2, 3 and 4 on samples (as shown in Figure 4.3). Average of these four measurements is taken as the Ra value for the sample in the particular polishing stage. Surface roughness measured by 2D profilometer before polishing on both samples showed that the granite is smoother than limestone. Figure 7.3 shows the variation of surface roughness paramter R_a in different polishing stages. Error bars shows the standard deviations of the measurements in each polishing stage. The initial R_a values before polishing for limestone and granite were 2.02 and 1.88 μm respectively. This shows that diamond saw cutting resulted relatively smooth surface for both of the samples. Therefore, SiC 400 was selected for the first polishing. The surface roughness of both samples decreased as the sample underwent each polishing stage. R_a values shows that in the initial polishing stages where the coarser grits where used, the decrease in roughness is higher than decrease in surface roughness with finer grit polishing stages such as 1000 SiC, 5μ and 3μ Aluminium Oxides. Three polishing stages with finer grits (1000 SiC, 5μ Aluminium Oxide, 3μ Aluminium Oxide) showed a uniform decrease in roughness until final polishing is reached.

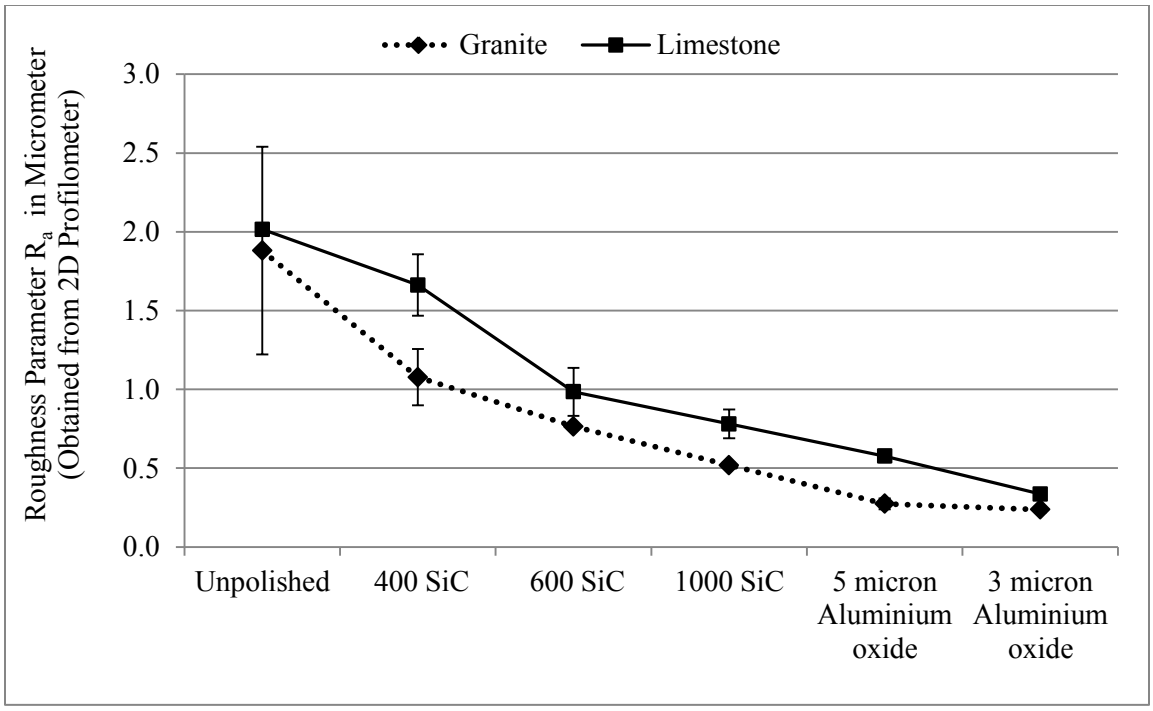

Figure 7.3 Variation of Surface Roughness Parameter R_a Obtained from 2D profilometer in Different Polishing Stages.

Figure 7.4 shows the variation of parameter R_z, with error bars showing the standard deviation of the measurements in each polishing stage. As the figure shows, R_z decreases as the polishing progresses. Along with that, standard deviation also decreased, showing the similar trend like R_a.

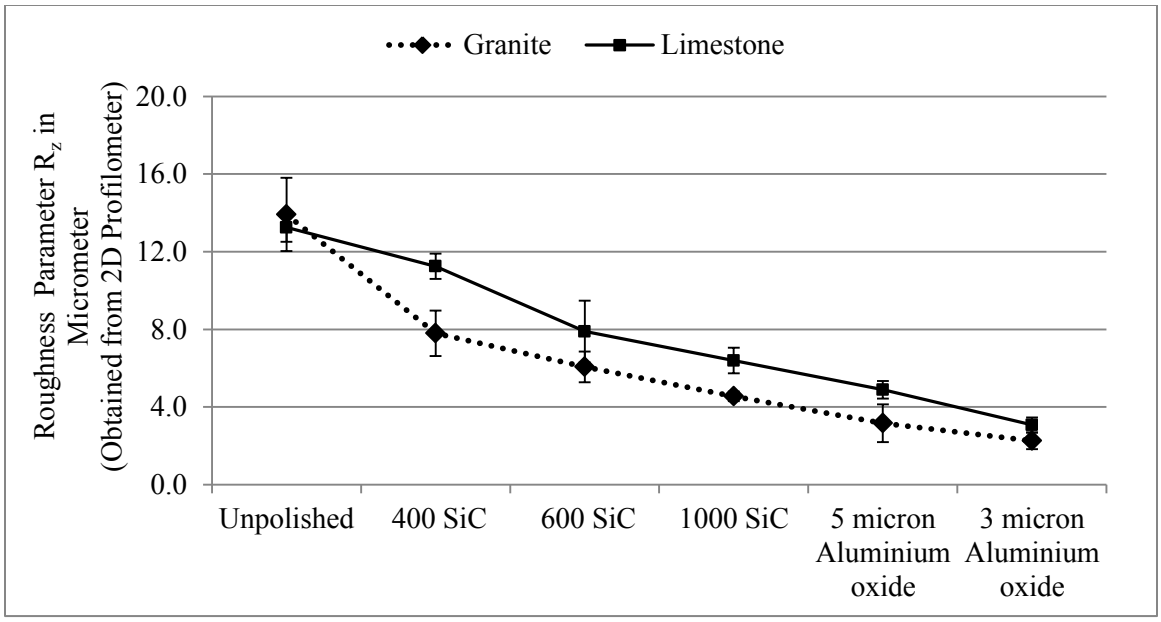

Figure 7.4 Variation Of Surface Roughness Parameter R_z Obtained from 2D profilometer in Different Polishing Stages.

Trend of the variation is similar to R_a for both the samples. The standard deviation also has decreased by the final polishing stage.

7.2.2 Three Dimensional Method of Surface Roughness Measurement (Non contact)

Using 3D optical profilometer Nanovea, two locations (numbered 1 and 5, as shown in Figure 4.3) of 1 cm x 1 cm on both samples are scanned. Ten R_a values were obtained from one 1 cm x 1 cm and average of ten values is reported as one R_a value for the area. This process is repeated for the second location as well. Average R_a of these two locations are calculated and given as R_a for the sample for the respective polishing stage. Figure 7.4 shows the variation of R_a with different polishing stages for granite and limestone samples. The results obtained from 3D optical profilometer were similar to that obtained from the 2D profilometer. The pattern of the change of the surface roughness of both samples showed decrease of surface roughness when polished with different silicon carbide grits as well as aluminium oxide powders. However for the granite, the

initial polishing stage doesnot show much of a reduction in the roughness. Also, roughness values measured by optical profilometer are different from that of 2D profilometer.

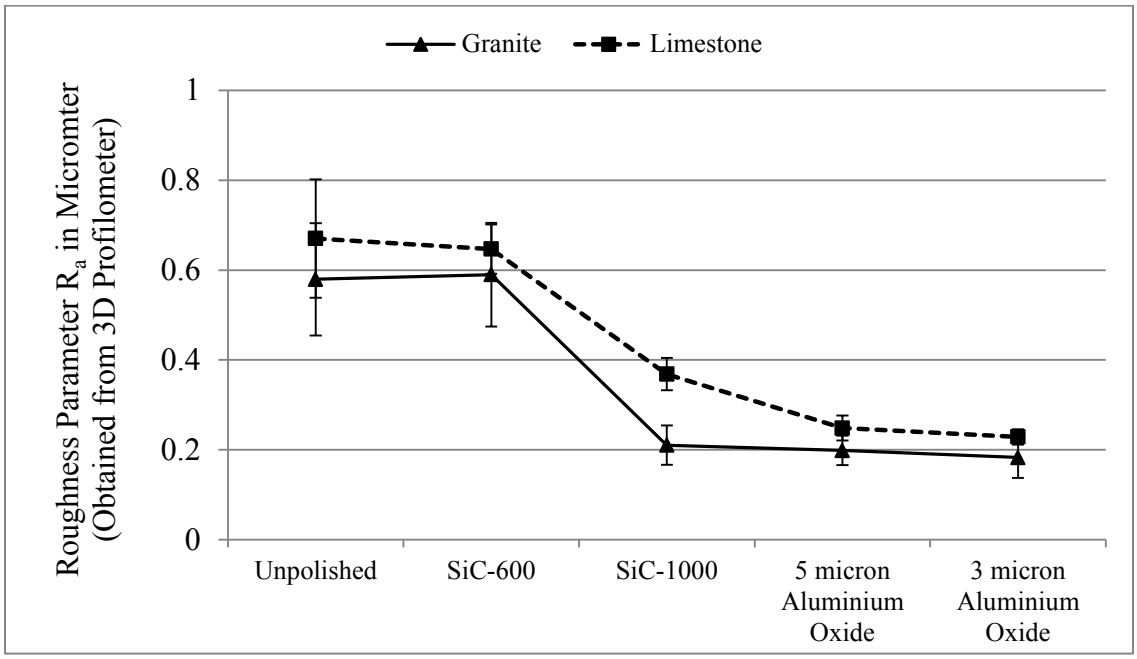

Figure 7.5 Variation Of Surface Roughness Parameter R_a,Obtained from 3D profilometer in Different Polishing Stages.

For the optical profliometer, the surface topography obtained by the software depends on the speed of the scanning specified. On a greater speed, the surface obtained is smoother than the real surface. This could be the reason between difference in the values of roughness parameters obtained from 3D and 2D profilometers. Figures 7.5 and 7.6 shows the topograhy of unpolished and polished surfaces of granite and limestone aggregate samples (1 cm x 1 cm area) , respectively.

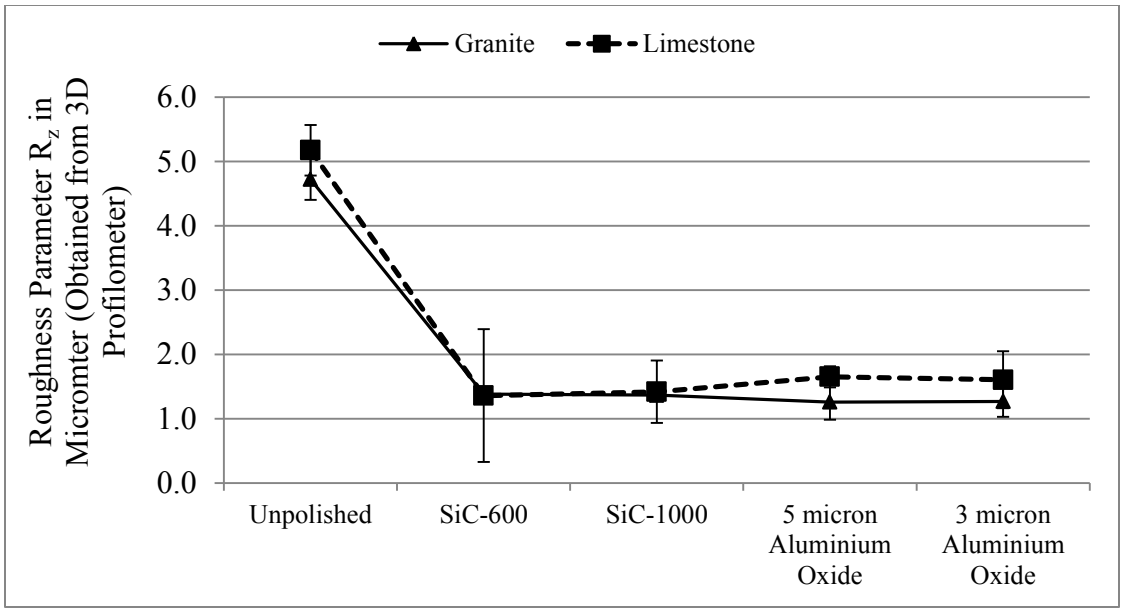

Figure 7.6 Variation Of Surface Roughness Parameter R_z,Obtained from 3D profilometer in Different Polishing Stages.

Figure 7.6 shows the variation of R_z, in different polishing stages. After polishing with 600 SiC, the standard deviation for granite shows an increase however, it further decreases until the final polishing stage. R_z for the limestone showed a slight increase after 1000 SiC and remained same until final polishing stage.

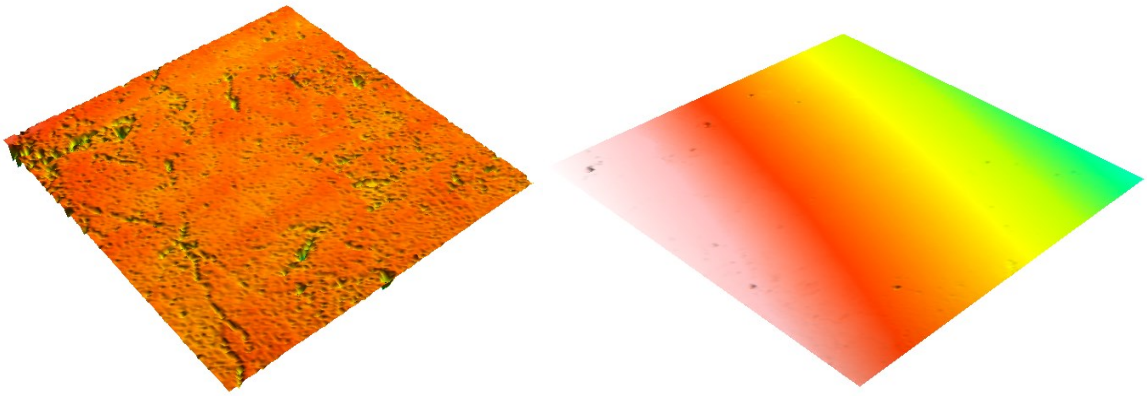

Figure 7.7 Images of Unpolished and Polished Surfaces of Granite Obtained from 3D Profilometer.

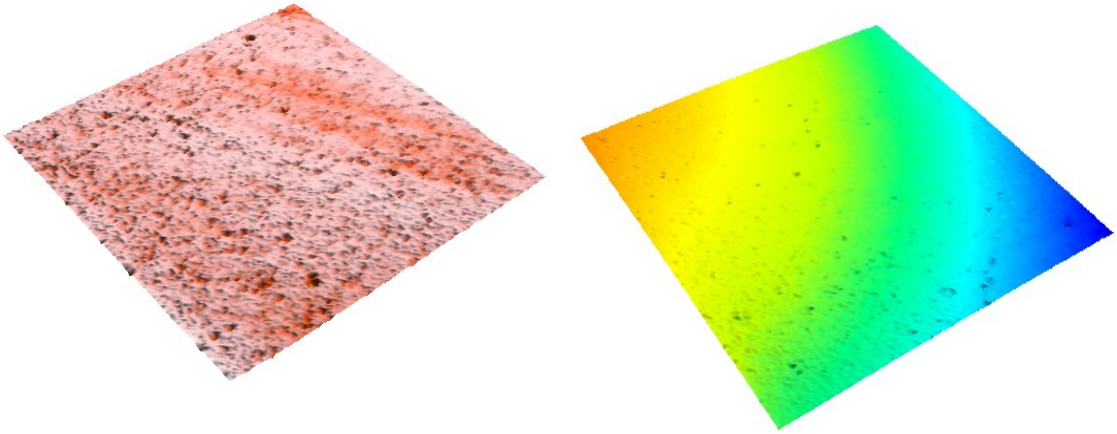

Figure 7.8 Images of Unpolished and Polished Surfaces of Limestone Obtained from 3D Profilometer

Well explained by the photographs, the surfaces became smooth after all the polishing stages. Also, it can be seen from the Figures (7.7 and 7.8) that limestone has a rougher surface than granite. This is well supported by the test results from 3D profilometer as well as 2D profilometer.

CHAPTER VIII

SURFACE ENERGY CALCULATIONS

Contact angles measured with three probe liquids (water, ethylene glycol and didiodomethane) are used for computing surface energy components of Mill Creek granite and Dolese Hartshorne limestone from Oklahoma. Using Equation 7 (which is reiterated below), surface energy components of probe liquid and corresponding contact angle, three simultaneous equations are formed.

$$(1 + cos\theta)\gamma_l = 2\left[\sqrt{\gamma_s^{LW}\gamma_l^{LW}} + \sqrt{\gamma_s^{+}\gamma_l^{-}} + \sqrt{\gamma_s^{-}\gamma_l^{+}}\right] \quad (7)$$

Since four components ($\gamma^{+}_{l}, \gamma^{-}_{l}, \gamma_l^{LW}, \gamma_l$) are known, only unknowns are the surface energy components of solids ($\gamma^{+}_{s}, \gamma^{-}_{s}, \gamma_s^{LW}, \gamma_s$). When contact angles were measured with three probe liquids on a solid surface, there will be three equations are formed with three unknowns. Average contact angles with three probe liquids from each polishing stage are used to calculate surface energy components in the particular polishing stage. These three equations are solved to find the surface energy components of Mill Creek granite and Dolese Hartshorne limestone. For this study, the equations are solved using an Excel spread sheet.

8.1 Dolese Hartshorne limestone

Surface energy components of Dolese Hartshorne limestone are computed using Equation 7. The variation of the base component, Lifshitz-Van der Waal's component and total surface energy are given in the Figure 8.1.

The change in contact angle values in different polishing stages are reflected in the variation of surface energy values. The total and Lifshitz Van der Waal's (LW) components of surface energy demonstrate similar pattern while the Lewis base component shows a different pattern.

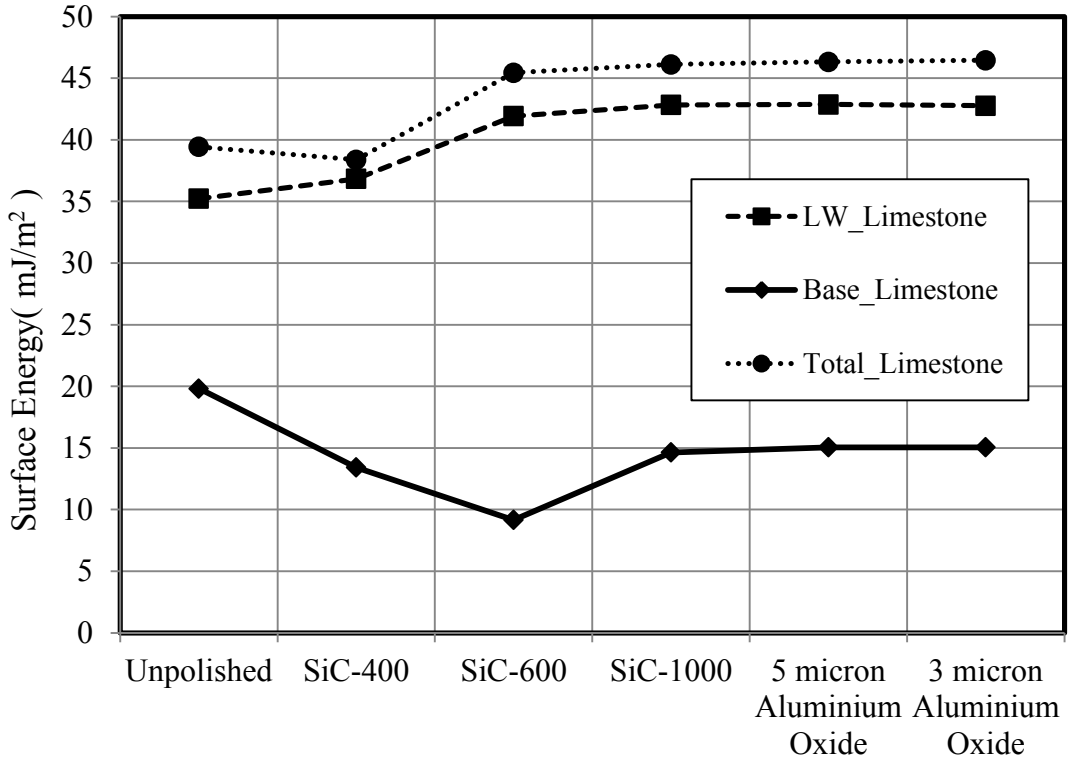

Figure 8.1 Variations of Total Surface Energy and Surface Energy Components In Various Polishing Stages.

Lewis acid components appear to be very small when compared with all the other components of surface energy. Table 8.1 shows the Lewis acid components of limestone sample obtained. In each polishing stage, contact angles are measured on five locations (locations are as described in Figure 4.3) on the limestone sample. Five repetitions were made on each of the locations and average of all the five repetitions are considered as contact angle for the particular polishing stage Appendix B shows the contact angle results and their corresponding standard deviations in various polishing stages.. For example, average of contact angle for water for the unpolished

sample is 71.73^{o} with a standard deviation of 5.17^{o}. From the Figure 8.1, it is evident that the variation in contact angles in each stage of polishing affected the surface energy values. When the polishing is performed on the sample, the contact angle decreased (variation of contact angles and respective standard deviations are explained in Chapter VII). For the limestone, the contact angle values using the probe liquid water did not show much variation over different polishing stages although there were more changes with respect to DIM and EG. From 1000 SiC polishing stage onwards, the contact angles of all the probe liquids did not show much variation. Corresponding to that, the surface energy components are also did not vary after 1000 SiC polishing stage.

Table 8.1. Lewis Acid Components of Surface Energy (mJ/m^2) for Dolese Hartshorne Limestone Sample in Different Polishing Stages.

	Unpolished	SiC-400	SiC-600	SiC-1000	5 micron Aluminium Oxide	3 micron Aluminium Oxide
Limestone	0.224	0.045	0.336	0.184	0.198	0.227
Granite	0.179	0.279	0.079	0.049	0.042	0.047

8.2 Mill Creek Granite

Surface energy components of Mill creek granite is computed at each polishing stage and the variations are shown in Figure 8.2. The contact angle measurements are obtained with sessile drop device were used for calculating the surface energy components. Contact angle measured at five locations (as shown in Figure 4.3), each location with five repetitions. Therefore, one contact angle is average of twenty five measurements. Variation of total surface energy, Lifshitz van der Waal's (LW) component and base component are similar as the polishing of the sample is completed. Lifshitz-van der Waal's component showed an increase in surface energy when

polished with SiC-400 and remained almost the same after several polishing stages. Unlike the change in Lifshitz-van der Waal's component, Lewis base component of surface energy varied considerable after first polishing of sample with SiC-400. However, the surface energy reduced after SiC 600 and remained without much change for further polishing stages. Lewis base component of surface energy on the rough surface is as low as 5.3 mJ/m^2 whereas after polishing with SiC-400, the base component of surface energy increased to 34.25 mJ/m^2 and kept on increasing until SiC-1000 polishing. The variation of total surface energy, Lifshitz van der Waal's component and Lewis base component of surface energy are given in Figure 8.2.

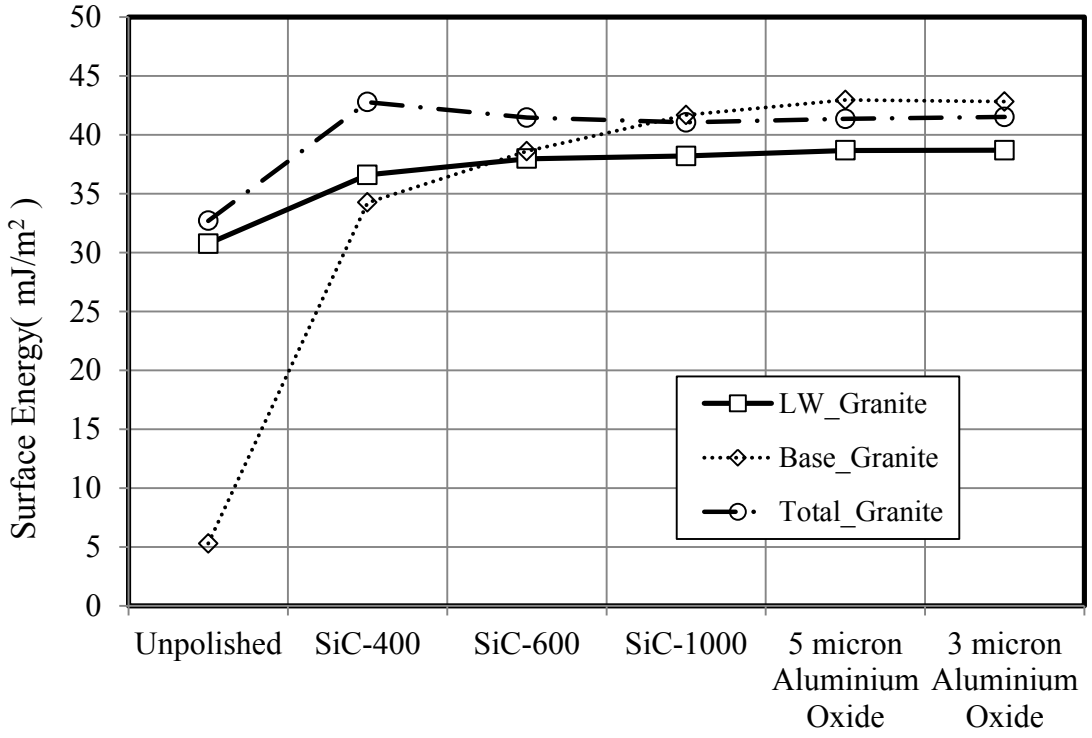

Figure 8.2 Variations of Total Surface Energy and Surface Energy Components of Mill Creek Granite in Various Polishing Stages.

The values of all the components of surface energy tend to stabilize after 1000 SiC polishing stage. Lewis acid components of surface energy were comparatively small. Table 8.2 represents the Lewis acid components of Mill Creek Granite at different polishing levels. Giese and van Oss

(2002) explain that for geologic materials like limestone and granite, the acid components and base component cannot co-exist in the same material. Since the Lewis acid component is related to the dryness of the material, the presence of acid component shows the existence of small moisture in the sample.

Table 8.2. Lewis acid (γ^+) Component of Surface Energy (mJ/m^2) for Mill Creek Granite at Various Polishing Stages.

Unpolished	SiC-400	SiC-600	SiC-1000	5 micron Aluminium oxide	3 micron Aluminium oxide
0.179	0.279	0.079	0.049	0.042	0.047

For both the limestone and granite aggregates, the total and Lifshitz-van der Waals components stabilizes and stay relatively constant from SiC-1000 polishing stage onwards. These trends coincide fairly well with the measured contact angle values using the sessile drop device (shown in Figure 7.1 and 7.2 of Chapter VII).

8.3 PG 64-22 Asphalt Binder

For the calculation of energy ratio and to compare the different asphalt mixes with limestone and granite, surface energy components PG 64-22 neat binder is considered. The surface energy values were computed from the contact angle measurements reported in thesis by Koc (2013). Using the sessile drop device, Koc (2013) determined a total surface energy of 36.53 mJ/m^2, Lifshitz van der Waal's component of 35.38 mJ/m^2, base component of 2.82 mJ/m^2, and acid component of 0.12 mJ/m^2 for the PG 64-22 asphalt binder from Muskogee, Oklahoma. Energy ratio and compatibility ratio at different polishing stages were computed for the asphalt mixes with Mill Creek granite and Dolese Hartshorne limestone and normalized energy ratios and compatibility ratios were plotted(Chapter IX, Section 9.2, Figure 9.4).

CHAPTER IX

ANALYSIS OF TEST RESULTS

9.1 Comparisons

In order to study the variation of contact angle measured on Mill Creek granite and Dolese Hartshorne limestone, test results from sessile drop device are compared. Also, the surface roughness parameter R_a results from two methods of surface roughness measurements are compared (i.e., 2D contact profilometer and 3D non-contact profilometer). In order to compare the surface roughness of the samples, a correlation is plotted with R_a values obtained in both methods. To evaluate the moisture sensitivity of the asphalt mix with granite and limestone, the energy ratio and compatibility ratio parameters are computed and compared.

9.1.1 Contact Angles of Limestone and Granite

Contact angle measured on rough surfaces of limestone and granite aggregates have shown that the probe liquids Water and DIM have returned larger contact angles on Mill Creek granite sample than on Dolese Hartshorne limestone sample. Also, for the contact angle measured with water on limestone and granite the standard deviation was 5.17 and 3.74^o respectively (Figure 7.1 and 7.2). When polished with 400 SiC, granite showed a drastic decrease in contact angle measured with water, from 84.88^o into 58.48 ^{o}. However, the standard deviation of the contact angle with water increased to 4.9^o. Figure 9.1 displays the contact angles with water EG and DIM on limestone and granite samples. For the limestone the contact angle value with water before polishing was 71.73^o which are lesser than the contact angle with water on granite (84.88^o).

However, after the final polishing is performed, contact angles obtained with water on limestone were 63.69°, which is greater than that of contact angle on smooth surface of granite. For granite, contacts angles with EG and DIM before polishing were 60.12 ° and 56.19 °. As the polishing progressed they decreased and the final values after 3 micron Aluminium oxide polishing were 33.343° and 41.78° respectively.

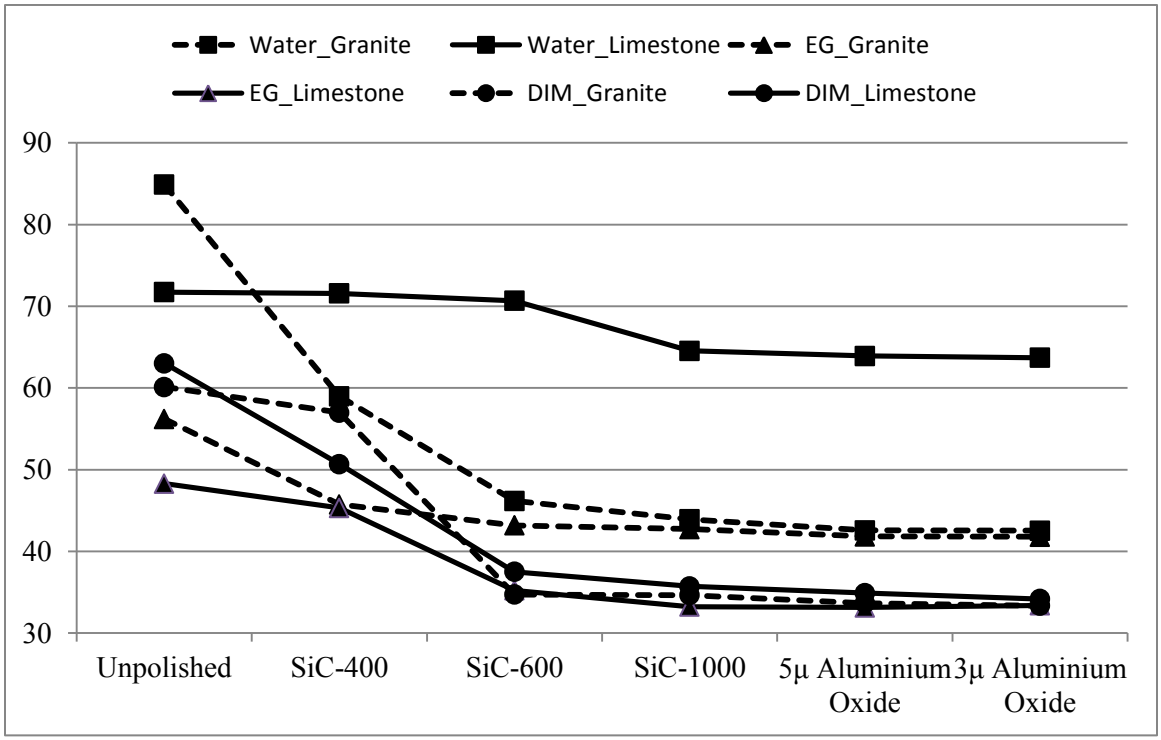

Figure 9.1 Variations of Contact Angles with Water, EG and DIM on Limestone and Granite in Various Polishing Stages.

Contact angle values for EG and DIM, on limestone before polishing were 63.02° and 48.28°. The contact angles values for EG and DIM after final polishing stage were 34.17° and 33.38°. From Figure 9.1, it can be seen that the contact angle value of DIM after final polishing on both samples were quite nearer whereas the contact angle with EG was different. Also, standard deviation of contact angle with all the probe liquids on both of the samples seemed to be decreasing after 600 SiC polishing stage (Figure 7.1 and Figure 7.2). In other words, the contact

angles became consistent and effect of change of surface roughness was reflected as decrease in standard deviation of contact angles.

9.1.2 Surface roughness of limestone and granite

Initial surface roughness measurement with both 2D and 3D surface roughness measurement methods revealed that Dolese Hartshorne limestone is rougher than granite. R_a value obtained after polishing with different silicon carbide grits and aluminum oxide powders on both of the samples showed that the surface became smoother. Surface roughness parameter R_a measured using 2D and 3D methods showed similar pattern. However, the R_a measured using 3D method was lower when compared to 2D R_a values. This could be attributed to the scanning speed of the 3D profilometer. When the scanning speed is increased, the surface profile obtained is comparably smoother than the actual surface. However, when the scanning speed is low, more time is taken for scanning the surface. Therefore the parameters calculated from same profile on a slower speed and higher speed will be different. The lower the speed of scanning, the better will be the roughness parameters obtained. Hence depending on the speed of the scanning the accuracy of the results may vary. This could be the reason why the R_a values obtained by 3D profilometer are different from that measured by 2D profilometer. However, the lower speed of scanning is not selected for the experiments in this study owing to more time consumption for the scanning.

Before polishing the granite sample, the R_a obtained using 2D and 3D methods were 1.88 and 0.58 μm respectively. On the other hand, results of 2D and 3D surface roughness measurement on the limestone showed R_a values of 2.01 and 0.67 μm respectively. However, after final polishing of the sample using 3 μm aluminium oxide powder, the R_a values obtained for granite by 2D and 3D method are 0.24 and 0.18 μm, respectively. For limestone the R_a values obtained by 2D and 3D method are 0.34 and 0.23 μm, respectively. This show that as the surface roughness decreases,

variation in the results from both methods are decreasing. Chand et al. (2011) compared results from an optical profilometer and stylus profilometer to study the roughness parameters on known roughness samples, and found that on smoother sample both methods of roughness measurements have closer values for roughness parameters. In other words, on a smoother sample 3D method of surface roughness could be as advantageous as the 2D method. In order to evaluate the association between Ra values from 2D and 3D methods a correlation is plotted with Ra values for both samples.

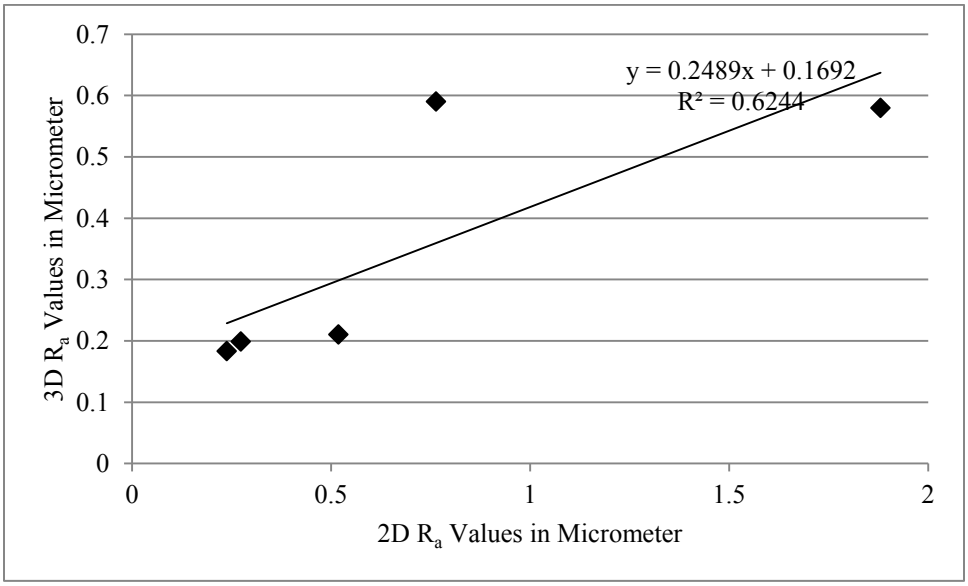

Figure 9.2 Correlation Between 2D and 3D R_a Values for Granite Sample.

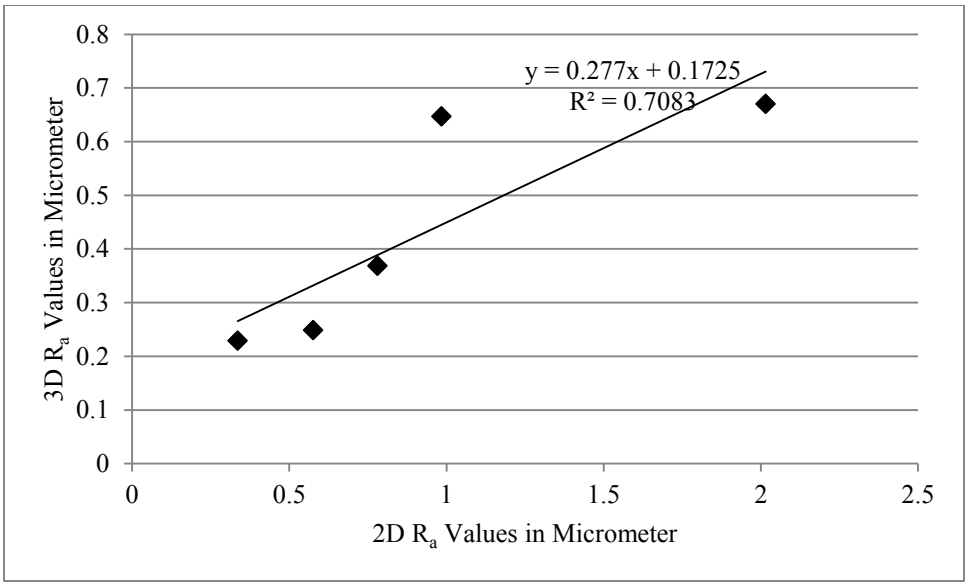

Figure 9.3 Correlation Between 2D and 3D R_a Values for Limestone Sample.

Correlation between 2D and 3D values is plotted using the R_a values obtained from unpolished, 600 SiC, 1000 SiC as well as 5 μ and 3 μ aluminium oxide polishing stages. The R^2 or the coefficient of determination obtained for granite and limestone were positive and were 0.624 and 0.708, respectively. This shows that even though the Ra values obtained by 2D and 3D methods were different, they both are fairly well correlated. Therefore either of the two methods could be used for obtaining the surface roughness changes for the samples.

9.1.3 Surface energy comparison of limestone and granite

Surface energy values are calculated using GVOC approach at each of the polishing stages, using the contact angles obtained from the sessile drop device (van Oss, 2002). Base component of surface energy of limestone and granite before polishing was 19.8 mJ/m^2 and 5.3 mJ/m^2, respectively. The base component of surface energy calculated for granite and limestone after final polishing were 15 mJ/m^2 and 42.8 mJ/m^2, respectively. As can be seen from Figure 8.1 in Chapter VIII, the base component of the limestone exhibits a different pattern from all the other surface energy components. Furthermore, the base component calculated for limestone decreased

when the sample is polished with the SiC-400 and SiC-600 polishing stages. Lewis acid component before polishing for the limestone was 0.224 mJ/m^2 and there was no considerable change in the acid component after polishing (0.227mJ/m^2). On the other hand, for the granite Lewis acid component was 0.179 mJ/m^2 before polishing and when the sample get polished, the acid component calculated was 0.047 mJ/m^2 . Lifshitz van der Waal's component for the limestone and granite before polishing were 35.2mJ/m^2 and 30.76 mJ/m^2 respectively (Figure 8.1, Chapter VIII). After the final polishing, the LW components calculated for the limestone and granite were 42.76 mJ/m^2 and 38.76 mJ/m^2 respectively. As shown in Figure 8.1 in Chapter VIII, total surface energy of the limestone and granite obtained before polishing is 39.4mJ/m^2 and 32.7mJ/m^2 respectively. After the final polishing stage, the total surface energy of the lime stone and granite increased to 46.5mJ/m^2 and 41.5mJ/m^2 respectively. Acid component as well as LW component of surface energy was greater for the limestone than granite whereas base component tend to be higher for the granite when compared to the limestone. However, total surface energy is higher for the limestone than granite. In order to estimate the moisture sensitivity of the samples in asphalt mix further analysis is conducted by computing work of adhesion in dry condition and work of adhesion in wet condition.

9.2 Energy Ratio and Compatibility Ratio Calculation

Energy ratio and Compatibility ratio are two parameters introduced by Bhasin and Little (2006) for evaluating moisture susceptibility of the asphalt mixture. Based on the surface energy values obtained for Mill Creek granite and Dolese Hartshorne limestone, the Energy ratio (ER) and Compatibility ratio (CR) for these aggregates with neat PG 64-22 asphalt binder were calculated. ER is the ratio of difference between adhesion in dry condition of the mix and cohesion of the binder to adhesion of mix in wet condition. CR is simply the ratio of adhesion in dry condition to adhesion in wet condition of the asphalt mix. ER and CR parameters were calculated for each polishing stages for both aggregates. Table 9.1 shows the work of adhesion in dry condition, work

of adhesion in wet condition, energy ratio and compatibility ratio for both limestone and granite samples in each polishing stage.

For the limestone, ER was as low as 0.06 with the rough surface which changed to 0.19 on polished sample. For granite, ER was 0.07 on the unpolished sample which was closer to the limestone ER. However, on polished granite sample the ER was 0.28 which is greater than limestone. The Gibbs free energy of adhesion (or work of adhesion) in dry condition (ΔG^{a}_{ikj}) for the limestone and binder combination is consistently higher than the work of adhesion between the granite and binder at the SiC-600 and higher levels of polishing stages. However, the difference between the dry work of adhesion between the two pairs is not large. Work of adhesion in wet condition or the work of debonding (ΔG^{a}_{ikj}) for the limestone and binder combination is higher in all the polishing stages above SiC-400 than the work of adhesion of the granite and binder combination.

In the ER calculation, the difference between dry adhesion (ΔG^{a}_{ij}) and cohesion (ΔG^{c}_{i}) shows the ability of the asphalt binder to wet aggregate surface (Little and Bhasin, 2006). In other words, this indicates the affinity of the asphalt binder to the aggregate surface or bonding between asphalt and aggregate. Therefore, when work of adhesion in wet condition (ΔG^{a}_{ikj}) is low, the ER is higher, which indicates the higher moisture resistance of asphalt mix. In other words, work of adhesion in wet condition is desired to be as low as possible, the limestone and binder combination could be susceptible to more moisture damage than granite and asphalt combination.

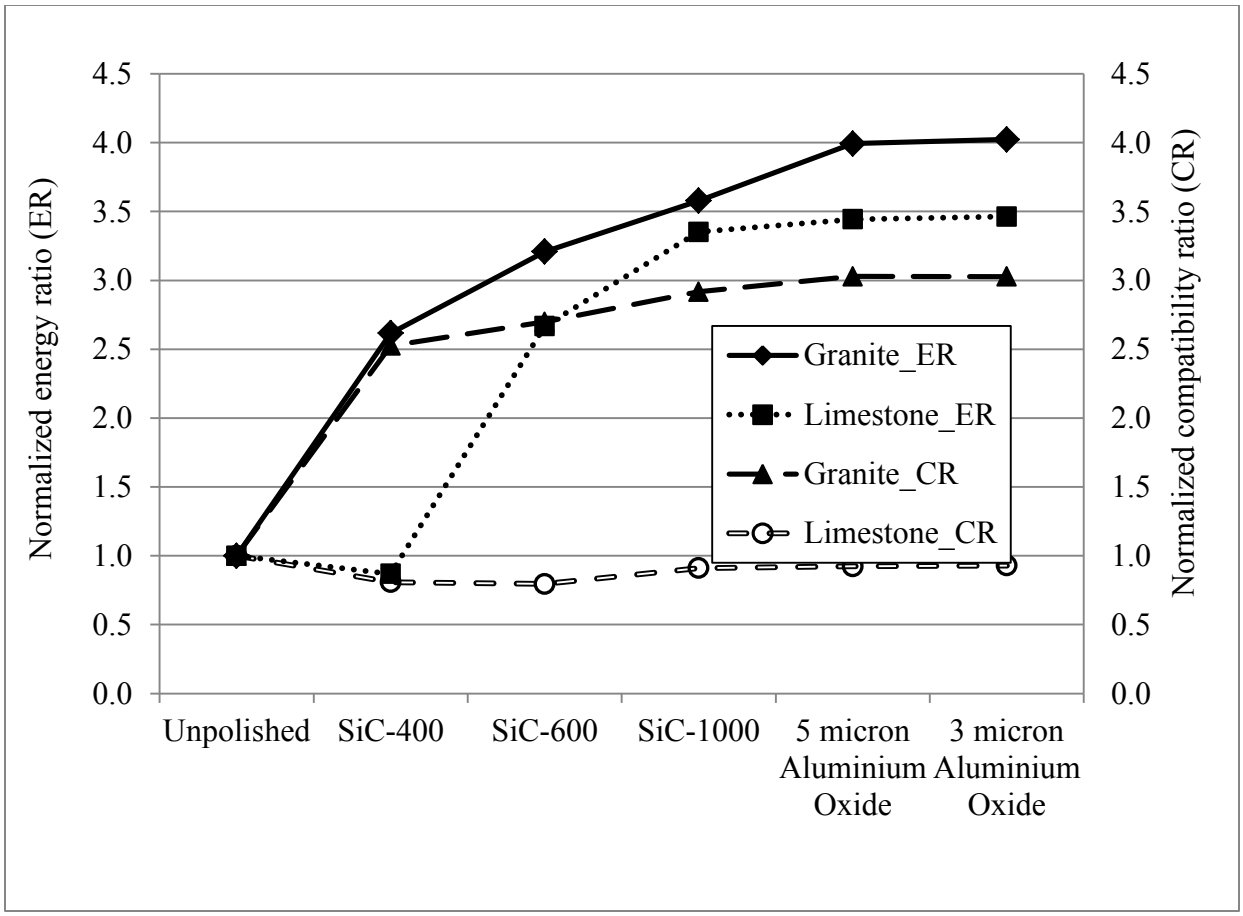

Figure 9.3 Normalized Energy and Compatibility Ratios for Mill Creek Granite and Dolese Hartshorne Limestone.

Table 9.1 Energy Ratio and Compatibility Ratio for Granite-Binder and Limestone-Binder mixes

Energy ratio (ER) and compatibility ratio (CR) for the Mill Creek granite with neat PG 64-22 asphalt binder and Dolese Hartshorne limestone with the same neat PG 64-22 asphalt binder									
Polishing Stage	Granite	Limestone	PG 64-22	Granite	Limestone	Granite	Limestone	Granite	Limestone
	ΔG^{a}_{ij} (mJ/m^2)		ΔG^{c}_{i} (mJ/m^2)	ΔG^{a}_{ikj} (mJ/m^2)		ER		CR	
Unpolished	68.99	75.28	73.06	–59.28	–39.71	0.07	0.06	1.16	1.90
SiC-400	77.81	75.45	73.06	–26.46	–49.25	0.18	0.05	2.94	1.53
SiC-600	78.56	81.08	73.06	–25.01	–53.78	0.22	0.15	3.14	1.51
SiC-1000	78.75	81.95	73.06	–23.19	–47.46	0.25	0.19	3.40	1.73
Al_2O_3-5μ	79.21	82.08	73.06	–22.47	–46.86	0.27	0.19	3.52	1.75
Al_2O_3-3μ	79.27	82.08	73.06	–22.50	–46.63	0.28	0.19	3.52	1.76

CHAPTER X

DISCUSSIONS

Contact angle measurements were performed on Dolese Hartshorne limestone and Mill Creek granite using three different probe liquids (water, EG and DIM). As it can be seen from Figures 7.1 and 7.2, the average contact angle for both the limestone and granite decreased with each finer polishing. In support to that, the surface roughness parameter R_a shows that the surface roughness decreased in each polishing stage for both of the samples after polishing. Further, the overall standard deviation of the average contact angles for all of the probe liquids showed a decreasing pattern. Also, after 1000 SiC polishing stage the overall average contact angles obtained were relatively consistent. Decrease in contact angle as the sample surface is polished can be explained by the change in surface roughness. Cassie (1948) explained that when there is surface roughness present on solids, the contact angles formed on the surface could entrap air without completely wetting the solid surface. In such cases, the contact angle exhibited by surfaces will not be the true contact angle of the solid. Further, Kwok and Neumann (1999) also states that when surface roughness is prominent, the contact angle formed on the surface of solid will reflect surface topography rather than the surface energy characteristics. Therefore it could be presumed that when the sample surface is polished it could result in reducing the topographical features (such as peaks and valleys) on the sample surface. As a result, the sample surface could have produced the representative (true) contact angle of the material.

Two different methods (2D contact profilometer and 3D non-contact optical profiloemeter) were used for measuring the surface roughness of the limestone and granite. Results from both

profilometers showed that sample surface became smoother after each polishing. However, the results from 3D profilometer were significantly different from the 2D profilometer results. Even though, the positive correlation between the two methods showed that both of the methods could be useful for measuring the surface roughness of the rock samples. The 2D surface roughness parameter R_a measured for the limestone and granite after polishing with 3 micron Aluminium Oxide were 0.34 and 0.24 μm, respectively. Using 3D profilometer the R_a obtained for limestone and granite were 0.22 and 0.18 μm, respectively. Therefore, both methods of roughness measurement showed that the surface roughness of the samples is below 1 μm. Giese and van Oss (2002) suggests that sessile drop contact angles should be measured on solid surface whose roughness is preferably less than 1 μm. Also, it should be noted that contact angles became consistent after 1000 SiC polishing where the surface roughness of granite and limestone were found to be 0.52 and 0.78 μm, which is in agreement with Giese and van Oss (2002). Surface energy values for the limestone and granite aggregate samples were calculated for each polishing stage using the GVOC approach. Figure 8.1 and Figure 8.2 explains the variation of surface energy of the limestone and granite respectively in different polishing stages. It was found that limestone possess higher total surface energy than granite. The difference between the total surface energy is around 5 mJ/m^2. The changes in contact angle values with respect to different polishing stages were reflected in the surface energy values as well. However, base component of limestone is significantly smaller than the base component of granite. Further, both samples exhibit acid component of surface energy in all the polishing stages. According to Giese and van Oss (2002), acid and base components will not co-exist on a completely dry material. Therefore, the small acid component shows the existence of moisture in the samples.

Previously, Bhasin (2006) estimated total surface energy of a limestone using Universal Sorption Device (USD) as 93.6 mJ/m^2. USD uses spreading pressure term in the calculation of surface energy. Bhasin and Little (2007) determined total surface energy of a granite using USD, and

found to be 48.8 mJ/m^2 , which is comparable to present study results on Mill Creek granite. Further, Wasiuddhin (2007) also determined total surface energy of a limestone (obtained from Sawyer, Oklahoma) using USD and found to be 219.9 mJ/m^2. Lytton et al. (2005) determined surface energy of granite and limestone using USD which is found to be 425.2 mJ/m^2 and 111.14 mJ/m^2. The differences in the surface energy determined using USD and sessile drop device could be due to the spreading pressure term. However, use of spreading pressure in the Young Dupre equation is still controversial. Nonetheless, Giese and van Oss (2002) suggested that when contact angles are greater than zero, it is not required to introduce a term like equilibrium spreading pressure. Fowkes et al. (1980) stated that when liquid surface energy is larger than solid surface energy, spreading pressure need not be considered. Further, Fowkes et al. (1980) explained that in certain cases involving hydrophilic surfaces, spreading pressure has some influence. However, van Oss (2002) suggests that even in such cases, it is not easy to evaluate with substantial degree of confidence. Furthermore, van Oss (2008) indicated that when liquid surface energy is less than solid surface energy, there exists a spreading pressure, but no contact angle. Additionally, Wu (1982) proposed that when contact angle is greater than 10^o the spreading pressure is insignificant. In a molecular model used in the study, Wu (1982) estimated that spreading pressure increases rapidly when contact angle approaches zero. Giese and van Oss (2002) estimated total surface energy of montmorillonite clay (59.8 mJ/m^2) with Column Wicking method. Montmorillonite is one of the most active geologic materials due to the presence of surface charges. Therefore, it is reasonable that the granite and limestone in present study showed a lesser total surface energy values than montmorillonite clay. Work of cohesion and work of adhesion in dry condition are calculated using the Equations 8 and 9 respectively. Table 9.1 explains the Gibbs free energy parameters for limestone, granite and PG 64-22 neat binder used in this study. It has been found that after the SiC 400 polishing stage, limestone has significantly high Gibbs free energy of adhesion in wet condition (wet adhesion, ΔG^a_{ikj}). As the

tendency of water to displace asphalt from the mix is characterized by the extent of free energy released, the lower the energy released the higher will be the moisture resistance (Bhasin and Little, 2007). Greater the work of debonding, greater will be the thermodynamic potential that drives the moisture damage. Hence, high wet adhesion is an undesirable quantity (Little and Bhasin, 2006). Further, Bhasin and Little (2007) explains that base component of aggregate also has a significant role in adhesion with water.

Energy Ratio (ER) and Compatibility Ratio (CR) are two parameters introduced by Bhasin and Little (2006) for evaluating moisture susceptibility of the asphalt mixture. Based on the surface energy values obtained for Mill Creek granite and Dolese Hartshorne limestone, CR and ER for these aggregates with neat PG 64-22 asphalt binder were calculated using the Equations 11 and 12 (Chapter III). From Table 9.1, it can be seen that, there is not much difference in ER values of granite and limestone before polishing (0.07 and 0.06 respectively). However, the ER obtained for limestone and granite after the final polishing is 0.19 and 0.28 respectively. CR for granite and limestone before polishing were 1.16 and 1.9 respectively. After final polishing, CR obtained for limestone and granite were 1.76 and 3.52 respectively, which were quite different from the initial trend. Even though, limestone has more surface energy than granite, the high adhesion in wet condition makes limestone more susceptible to moisture damage than granite sample. The energy parameters ER and CR are indicators of the sensitivity of asphalt mix towards moisture (Little and Bhasin 2006). For instance, Hefer et al. (2006) compared limestone and PG 64-22 along with modified asphalt mixes using CR calculations along with Hamburg test results on the same asphalt mixes. The results obtained from Hamburg tests compared with CR (2.01) showed that the asphalt mix with higher compatibility ratio and minimum work of adhesion in wet condition, displayed the minimum rut depth. In a study conducted by Bhasin and Little (2007) for characterization of different types of aggregates with modified and non- modified bitumen, compatibility ratios were used to compare the mixes, which showed that the CR is capable of

demonstrating a convenient way to predict moisture sensitivity of asphalt mixes. Further, Little and Bhasin (2006) compared energy parameters for a number of asphalt mixes along with test results from dynamic mechanical Analyzer for the mixes and results showed that the energy parameters could be used as a material selection tools for identifying moisture sensitive asphalt mixes. Comparison of results between the limestone and granite mixes from present study also indicates the same. Therefore, by using ER and CR as moisture sensitivity predicting tools for asphalt mixes, better compatible aggregate and asphalt could be identified and thereby moisture damage could be minimized.

CHAPTER XI

CONCLUSIONS

Contact angles and surface roughness were measured on flat specimens of Dolese Hartshorne limestone and Mill Creek granite. Successive polishing was performed on the samples using different grades of silicon carbide abrasives as well as two different aluminum oxide powders. The roughness measurements conducted using the 2D and 3D method revealed that the surface roughness reduced significantly from the first polishing stage to the final polishing stage. Even though the roughness parameter R_a was different for both 2D and 3D methods of measurement, the correlation plotted between the two methods showed that both methods could be helpful for quantifying the surface roughness. Also, compared to 2D method, 3D profilometer can give a number of roughness parameters for the detailed analysis of the surface roughness as well as the topographical image of the surface can also be obtained from 3D profilometer. Average contact angle obtained on the rock surface showed that the contact angle progressively decreased over several polishing stages. The standard deviation of the contact angles also decreased as the polishing approached final stage. The results from the present study indicate that surface roughness influence the contact angle measurement significantly. Thereby, the surface energy calculations will also be affected by the surface roughness as well. Therefore, polishing should be employed to reduce surface roughness. However, it is also evident from the study that after SiC 1000 the contact angles were relatively consistent and standard deviation also reduced. This indicates that only a certain degree of polishing is required to obtain consistent contact angles on aggregate surfaces. Further, roughness measurements combined with literature reviews shows

that roughness should be below 1 μm to obtain consistent contact angle results Surface energy components were calculated for both of the limestone and granite samples using GVOC approach. Average contact angle obtained in each polishing stage is used for computing the surface energy components. The results showed that the limestone possess more surface energy than the granite. However, the difference between total surface energy of limestone and granite were not large. Also, surface energy computed from sessile drop device is significantly different from that computed using Universal Sorption Device. This difference could be attributed with the spreading pressure term employed in the USD surface energy calculations. However, surface energy results obtained from this study are comparable to the results obtained by Koc (2013). Further, surface energy calculated on granite and limestone in this study is found to be comparable with the results obtained on geological materials as clays by Giese and van Oss (2002) and Yildirim (2001). Using the surface energy components, the limestone and granite are paired with PG 64-22 neat asphalt binder to find work of adhesion in dry condition, work of adhesion in wet condition and work of cohesion of the binder. It has been found that in wet condition, the work of adhesion is large for limestone. Energy Ratio and Compatibility Ratios were calculated for evaluating the sensitivity of the limestone with PG 64-22 neat binder as well as granite and PG 64-22 asphalt binder. The findings from the results of compatibility and energy ratios revealed that granite and PG 64-22 produced a better moisture resistant mix than limestone and PG 64-22 binder.

CHAPTER XII

RECOMMENDATIONS

Results from the present study imply that the sessile drop device can be used successfully for direct measurements of contact angle on flat solid surfaces. Roughness measurement from both 2D and 3D methods suggests that there are some differences from the results obtained. In order to optimize the roughness measurements, more study should be performed using 3D method with different speed so that the scanning speed suitable for different aggregates can be identified. Also, 2D and 3D roughness measurements could be performed on different types of aggregate samples in order to ensure the reproducibility of the results.

Even though, the surface energy parameters computed for the granite and limes stone aggregate samples in this study did not have compliance with that of USD results, they were comparable with result found in the literature (Giese and van Oss (2002), Yildrim (2001)). However, this study concentrates on only two types of aggregates and only one type of asphalt binder. Each time the sample is polished, surface polishing exposes relatively new surface area especially when the aggregate material is heterogeneous in mineral content. This could affect contact angle formed on the sample, depending on the surface energy. Therefore, the effect of aggregate mineralogy in ER and CR could be studied in detail. Hence, further studies should be performed on a number of aggregates as well as asphalt samples so that more susceptible combination of aggregates and asphalt can be identified

REFERENCES

1. APA (Asphalt Pavement Alliance). (2013). Asphalt pavement - America rides on us. http://asphaltroads.org/documents/Asphalt_White_Paper_doc.pdf. Assessed on Jan 5, 2013.
2. Aveyard, R., and Haydon, D. A. (1973). "An Introduction to the Principles of Surface Chemistry." 1st edition. Cambridge University Press.
3. Bhangham, D. H., and Razouk, R. I. (1937). "Adsorption and the Wettability of Solid Surfaces." *Transaction of Faraday Society,* 33, 1459-1463.
4. Bhasin, A. (2006). "*Development of Methods to Quantify Bitumen-Aggregate Adhesion and Loss of Adhesion Due to Water*." Ph.D. Dissertation, Texas A&M University, College Station, Texas.
5. Bhasin, A., and D.N. Little. (2007). "Characterization of Aggregate Surface Energy Using the Universal Sorption Device", *Journal of Materials in Civil Engineering*. Vol.19, 634-641.
6. Bico, J., Thiele, U. and Quere, D. (2002). "Wetting of Textured Surfaces." *Colloids and Surfaces A: Physicochemical and Engineering Aspects* Vol. 206, 41-46.
7. Busscher, H. J., Kip, G., A., M., Silfout A. V., and Arends, J. (1986), "Spreading Pressures of Water and n-Propanol on Polymer Surfaces." *Journal of colloid Interface Science*, Vol. 114, No.2, 307-313.
8. Busscher, H. J., Van Pelt, A. W. J., De Boer, P., De Jong, H. P., and Arends, J. (1984). "The Effect of Surface Roughening of Polymers on Measured Contact Angles of

9. Liquids." *Colloids and Surfaces*, Vol 9. 319-331.
10. Cassie, A. B. D. (1948). "Contact angles." *Discussions of Faraday Society*. 3: 11-16.
11. Chand, M., Mehta, A., Sharma, R., Ojha V., N., and Chaudhury K., P. (2011). "Roughness Measurement using Optical Profiler with Self- reference Laser and stylus Instrument – A Comparative Study." *Indian Journal of Pure and Applied Physics,* Vol. 49, 335-339.
12. Cheng, D. (2002). "Surface Free Energy of Asphalt-Aggregate Systems and Performance Analysis of Asphalt Concrete Base on Surface Free Energy," Ph.D. Dissertation, Texas A&M University, College Station, Texas.
13. Cheng, D. X., Little D., Lytton R. L., and J. C. Holste. (2003) "Moisture Damage Evaluation of Asphalt Mixtures by Considering Both Moisture Diffusion and Repeated-Load Conditions." *Journal of Transportation research Board*, Vol. 1832, 42-49.
14. Ebril H. Y. (2006). "Surface Chemistry of Solid and Liquid Interfaces." Wiley, New York.
15. Eick, J. D., Good, R. J., and Neumann, A. W. (1975). "Thermodynamics of Contact Angles II Rough Solid Surfaces." *Journal of Colloid and Interface Science.* Vol. 53, No. 2, 235-248.
16. Fowkes, F., M., McCarthy, D., C., and Mostafa, M., A. (1980). "Contact Angles and the equilibrium Spreading pressures of Liquids on Hydrophobic Solids." *Journal of colloid Interface Science,* Vol. 78, no. 1, 200-206.
17. Gadelmawla, E. S., Koura, M. M., Maksoud, T. M. A., Elewa, I. E. M., and Soliman., H. H., (2002). "Roughness parameters." *Journal of Material Processing Technology*, Vol. 123, No. 1, 133-145.
18. Gao, L., and McCarthy, T. J. (2006). "Contact Angle Hysteresis Explained." Langmuir. Vol. 22, 6234-6237.

19. Good, R.J. (1992). "Contact Angle, Wetting and Adhesion: A Critical Review". Journal of Adhesion Science and Technology, Vol 6(12), pp. 1269-1302.
20. Gorgulu, K., and Ceylanoglu, A. (2008). "Evaluation of Continuous Grinding Test on Some Marble and Limestone Units with Silicon Carbide and Diamond Type Abrasives." *Journal of Material Processing Technology*, Vol. 204, pp. 264-268.
21. He, B., Lee, J., and Patankar, N. A. (2004). "Contact Angle Hysteresis on Rough Hydrophobic Surfaces." *Colloids and Surfaces A: Physicochemical and Engineering Aspects,* 248: 101–104.
22. He, B., Patankar, N. A., and Lee, J. (2003). "Multiple equlibirum droplet shapes and design criterion for rough hydrophilic surfaces." Langmuir 19: 4999-5003.
23. Hefer, A. W., A. Bhasin, and Little, D. N. (2006). "Bitumen Surface Energy Characterization Using a Contact Angle Approach." *Journal of Materials in Civil engineering*, Vol. 18, pp. 759-767.
24. Howson, J. E. (2011). "*Relationship Between Surface Free Energy and Total Work of Fracture of Asphalt Binder and Asphalt Binder Interfaces*." PhD Dissertation, Texas A&M University, College Station, Texas.
25. Howson, J., Masad, E., Bhasin, A., Little D., and Lytton, R. (2011). "Comprehensive Analysis of Surface Free Energy of Asphlats and Aggregates and the Effects of Changes in pH." *Construction and Building materials*, 25, 2554-2564.
26. Kiggundu, B. M., and Roberts, F. L. (1988). "The Success/Failure of Methods Used to Predict the Stripping Propensity in the Performance Of Bituminous Pavement Mixtures."
27. Koc, M.(2013) "*Development of Testing Protocols for Direct Measurements of Contact Angles on Aggregate and Asphalt Binder Surfaces Using a Sessile Drop Device."* MS Thesis, Oklahoma State University, Stillwater, Oklahoma.

28. Koc, M., and R. Bulut. (2013). "Assessment of Sessile Drop Device and New Testing Approach for Measuring Contact Angles on Aggregates and Asphalt Binders." *ASCE Journal of Materials Engineering.* (In Press)
29. Kwok, D. Y. and Neumann, A. W. (1999). "Contact Angle Measurement and Conatct Angle Interpretation. Advances in Colloid and Interface Science." Vol. 81,167-249.
30. Kwok, D., Y., Gietzelt , T., Grundke, K., Jacobasch H.-J., and Neumann, A., W. (1997)."Contact Angle Measurements and Contact Angle Interpretation. 1. Contact Angle Measurements by Axisymmetric Drop Shape Analysis and a Goniometer Sessile Drop Technique." *Langmuir*, *13* (10), 2880–2894.
31. Little, D., and Bhasin, A.(2006) *Using Surface Energy Measurements to Select Materials for Asphalt Pavements*, NCHRP web only document 104.
32. Lobato, E., M., C. (2004). "Determination of Surface Free Energies and Aspect Ratio of Talc." Ms. Thesis, Virginia Polytechnic Instute and State University, Blacksburg, Virginia.
33. Lytton, R.L., Masad, E., Zollinger, C., Bulut, R., and Little, D.N. (2005). "Measurement of Surface Energy and Its Relationship to Moisture Damage." TxDOT Report Number 0-4524-2. FHWA, Texas Transportation Institute, Texas A&M University, College Station, Texas.
34. Majidzadra, K., and Brovold, F. N. (1968). "State of Art: effect of Water on Aggregate Mixtures." *Special Rep., Highway Research Board,* Washington D.C.
35. Miller, C., Little, D., N., Bhasin, A., Gardner, N. and Herbert, B. (2012). "Surface Energy Characteristics of Natural Minerals and Their Impact of Aggregate-Bitumen Bond Strengths and Asphalt Mixture Durability." Transportation Research Record, 45-55.
36. NAPA (National Asphalt Pavement Association). *Asphalt Pavement Overview*. (2013). https://www.asphaltpavement.org/index.php?option=com_content&view=article&id=14&Itemid=33. Accessed July 6, 2013.

NCAT Rep. No. 88-02, National center for Asphalt Technology, Auburn, Ala.

37. Onda, T., Shibuichi, S., Satoh, N., and Tsujii, K. (1996). "Super-Water-Repellent Fractal Surfaces." *Langmuir*, 12: 2125–2127
38. Patankar, N. A. (2003). "On the modeling of hydrophobic contact angles on rough surfaces." *Langmuir* 19: 1249-1253.
39. Good., R., J (1952). "A Thermodynamic Derivation of Wenzel's Modification of Young's Equation for Contact Angles; Together with a Theory of Hysteresis[1] ". *Journal of American chemical Society*, 74, 5041.
40. Rhee, S., K. (1973). "A Method for Determining Surface Energy of Solids*." Journal of Material science engineering.* 11, 311-318.
41. Tamai, Y. and Aratani, K. (1972). "Experimental Study of The Relation Between Contact Angle And Surface Roughness." *The Journal of Physical Chemistry.* Vol. 76. No. 22.
42. Tavana, H. and Neumann, A. W.(2007) "Recent Progress in the Determination of Solid Surface Tensions from Contact Angles." *Advances in Colloid Interface Science*, 132:1-32.
43. Terrel, R. L. and Al-Swailmi, S. (1994). Water Sensitivity of Asphalt-Aggregate Mixes: Test Selection. Strategic Highway Research Program (SHRP-A-403), National Research Council, Washington, DC.
44. van Oss C. J. (2008). *The Properties of Water and Their Role in Colloidal and Biological Systems.* Academic Press, Oxford.
45. van Oss, C. J. (1988). "Interfacial Liftshitz-van der Waals and Polar Interactions in Macroscopic Systems." *Chemical Reviews*, Vol. 88, 927-941.
46. van Oss, C. J. (2006). "Interfacial Forces in Aqueous Media." 2nd edition, Marcel Dekker, Inc., New York.

47. van Oss, C.J. (2002).”Use of the Combined Lifshitz-van der Waals and Lewis Acid-base Approaches in Determining the Apolar Contributions to Surface and Interfacial Tensions and Free Energies.” *Journal of Adhesion Science and Technology*, Vol. 16, 669-677.

48. Wasiuddin, N., M. (2007). “*Effect of Additives on Surface Free Energy Characteristics of Aggregates and Binders in Hot Mix Asphalt*.” Ph.D. Dissertation, University of Oklahoma, Norman, Oklahoma.

49. Wasiuddin, N., M., Zaman, M., and O’Rear, E., A. (2008). “Effect of Sasobit and Aspha-Min on Wettability and Adhesion Between Asphalt Binders and Aggregates.” Transportation Research Record No. 2051, Transportation Research Board, Washington, D.C., 80-89.

50. Wenzel, R., N. (1936), “Surface Roughness and Contact Angle.” *Journal of Physical Chemistry*, 1949, *53* (9), 1466–1467.

51. Wu, S. (1982). “Interfacial Thermodynamics in Polymer Interface and Adhesion.” Marcel Dekker, New York.

52. Yavuz, H., Ozkahraman, T., and Demirdag, S. (2011). “Polishing Experiments on Surface Quality of Building Stone Tiles.” Construction and Building Materials, Vol. 25, Issue 4, 1707–1711.

53. Yildirim, I. (2001). “Surface Free Energy Characterization of Powders.” Ph.D. Dissertation, Virginia Polytechnic Institute and State University, Blacksburg, Virginia.

54. Yilmaz, A., and Sargin, S. (2012). “Water effect on Deteriorations of Asphalt Pavements.” The Online Journal of Science and Technology, Vol. 2 Issue 1.

55. Zhou, X., B., and De Hosson, J., Th., M. (1995) “Influence of Surface Roughness on Wetting Angle” *Journal of Material Research Society*. Vol.10 (8). 1984-1992.

APPENDICES

Appendix A:

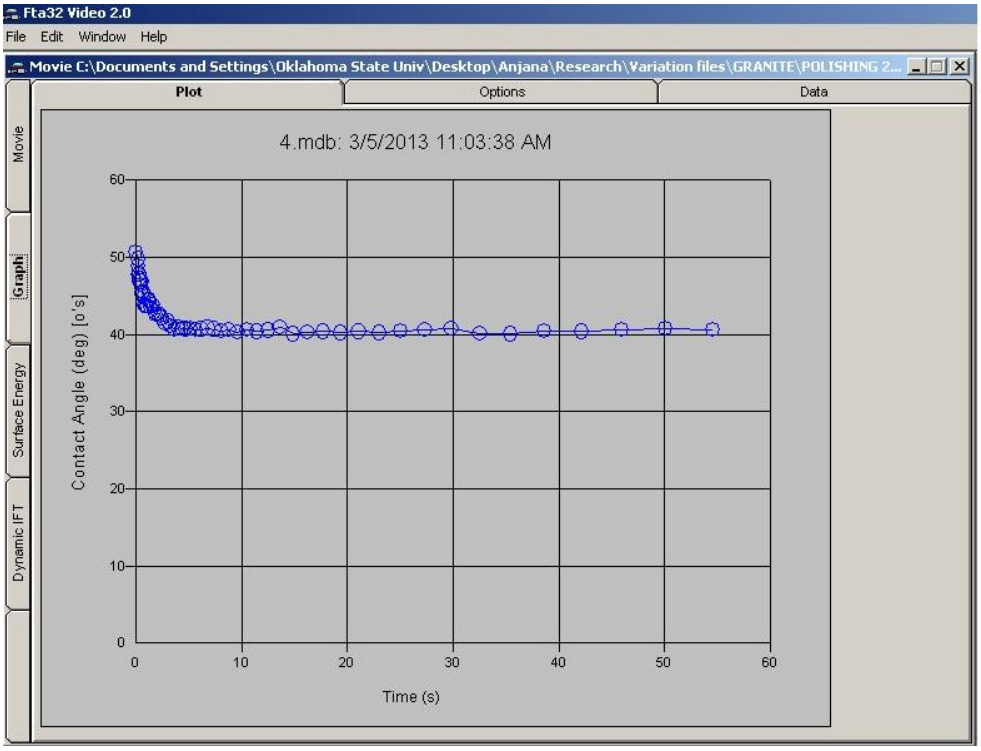

Figure A.1 Plot Obtained Between Time Elapsed and Contact Angle (Output from Sessile Drop Device).

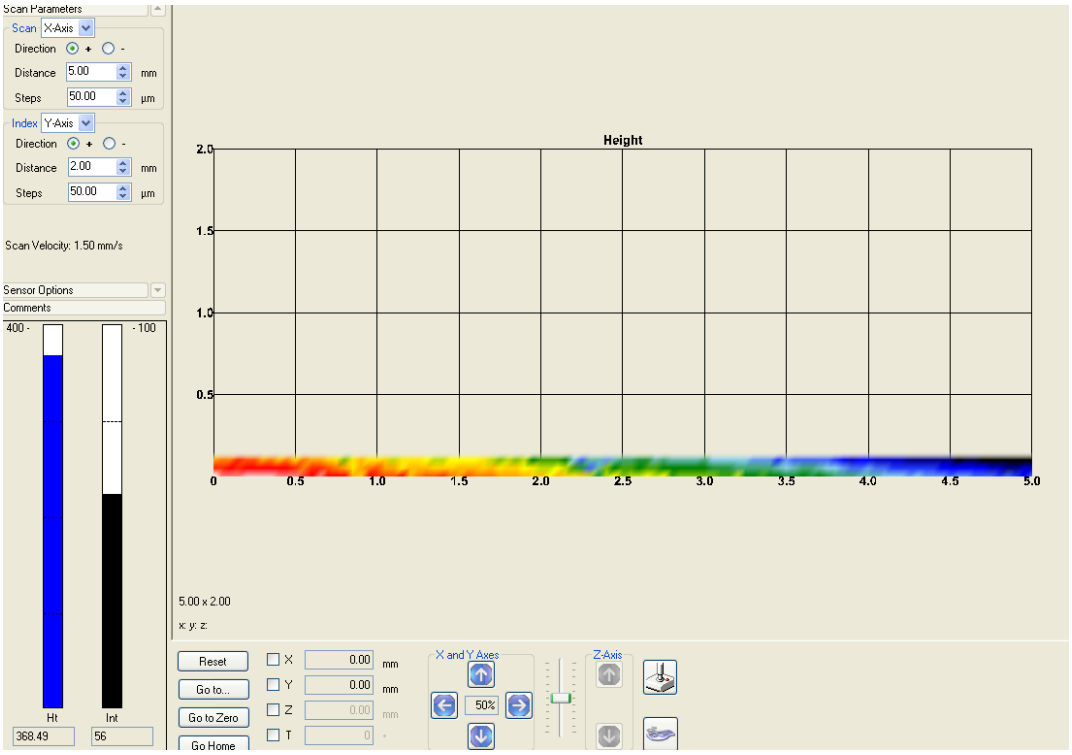

Figure A.2 Input Window of Nanovea Optical profliometer.

ISO 4287			
Amplitude parameters - Roughness profile			
Rp	1.321	µm	*Rp: Maximum Peak Height of the roughness profile.*
Rv	3.402	µm	*Rv: Maximum Valley Depth of the roughness profile.*
Rz	4.723	µm	*Rz: Maximum Height of roughness profile.*
Rc	2.017	µm	*Rc: Mean height of the roughness profile elements.*
Rt	12.99	µm	*Rt: Total Height of roughness profile.*
Ra	0.6272	µm	*Ra: Arithmetic Mean Deviation of the roughness profile.*
Rq	0.9233	µm	*Rq: Root-Mean-Square (RMS) Deviation of the roughness profile.*
Rsk	-1.361		*Rsk: Skewness of the roughness profile.*
Rku	7.202		*Rku: Kurtosis of the roughness profile.*
Material Ratio parameters - Roughness profile			
Rmr	1.518	%	*Rmr: Relative Material Ratio of the roughness profile.*
Rdc	1.076	µm	*Rdc: roughness profile Section Height difference*

Figure A.3 Typical Output from 3D profilometer, Showing the Roughness Parameters.

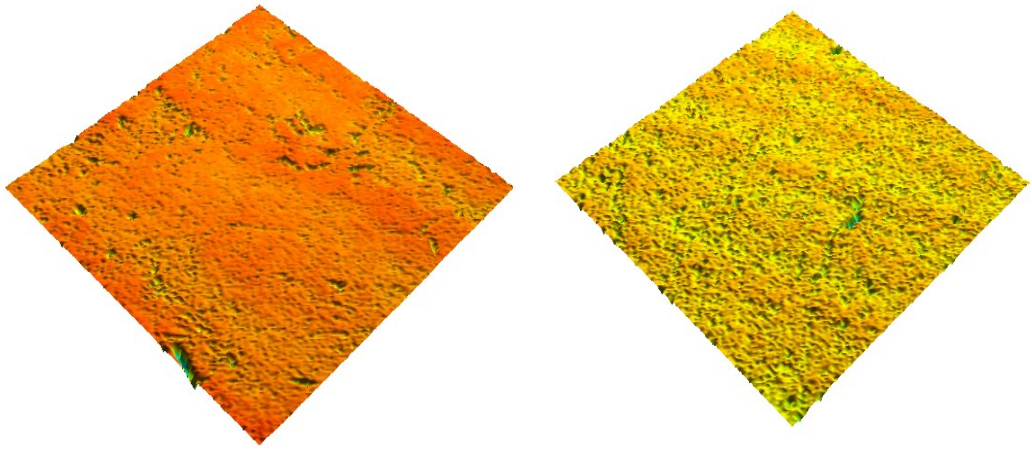

Figure A.4 Images of Unpolished Surfaces of Granite and Limestone (Location 5) Obtained from 3D Profilometer.

Figure A.5 Images of Granite and Limestone Surfaces Polished with 600 SiC of (Location 1) Obtained from 3D Profilometer.

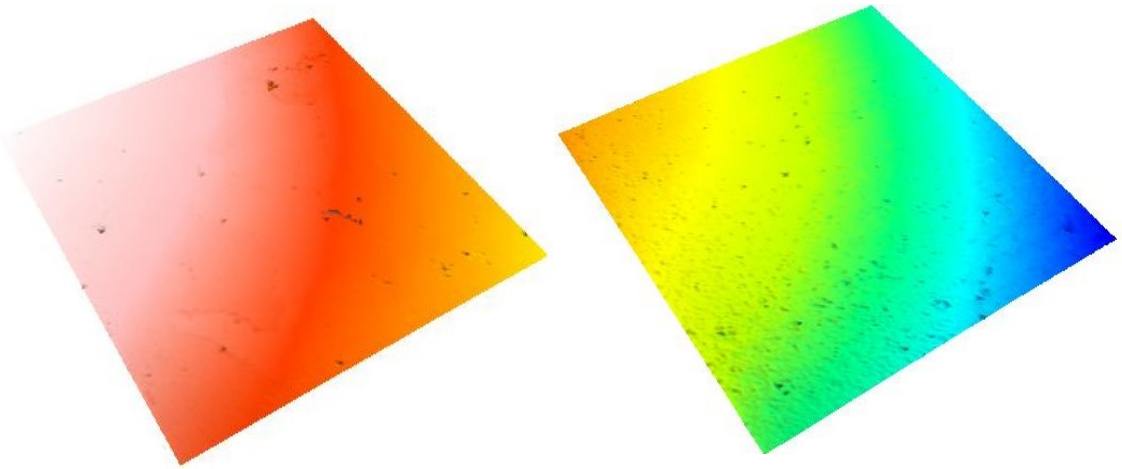

Figure A.6 Images of Granite and Limestone Surfaces Polished with 3µ Aluminium Oxide of (Location 5) Obtained from 3D Profilometer.

Appendix B:

Contact Angle and Surface Energy Values on Granite and Limestone

Table B.1 Contact Angle with Water on Mill Creek Granite Before polishing

Location	Set 1	Set 2	Set 3	Set 4	Set 5
1	85.77	83.37	79.96	83.59	80.14
2	81.88	82.55	81.03	78.84	84.49
3	85.24	83.66	84.00	87.17	88.18
4	89.33	80.36	89.92	85.73	81.34
5	86.18	92.81	87.63	91.20	87.77
Average	85.68	84.55	84.51	85.31	84.38
Overall average					84.88
Overall std. deviation					3.74

Table B.2 Contact angle with EG on Mill Creek Granite before polishing

Location	Set 1	Set 2	Set 3	Set 4	Set 5
1	58.85	57.93	58.62	55.82	63.54
2	57.98	59.79	63.61	56.48	62.42
3	59.09	61.66	56.99	65.29	58.73
4	64.54	58.91	62.01	58.31	58.60
5	60.63	64.02	61.08	63.44	54.74
Average	60.22	60.46	60.46	59.87	59.60
Overall average					60.12
Overall std. deviation					2.91

Table B.3 Contact angle with DIM on Mill Creek Granite before polishing

Location	Set 1	Set 2	Set 3	Set 4	Set 5
1	49.646	54.227	61.417	56.695	57.859
2	52.182	58.005	62.629	57.224	55.885
3	50.986	55.393	54.731	61.817	58.956
4	53.314	56.358	55.558	60.213	53.636
5	50.155	50.273	59.383	58.247	60.171
Average	51.26	54.85	58.74	58.84	57.30
Overall average					56.20
Overall std. deviation					3.77

Table B. 4 Contact Angle with Water on Mill Creek Granite after 400 SiC Polishing

Location	Set 1	Set 2	Set 3	Set 4	Set 5
1	55.77	60.66	51.90	60.08	59.69
2	62.16	56.43	67.86	60.73	59.71
3	52.05	67.86	55.20	57.78	53.37
4	67.75	63.18	57.95	58.40	56.60
5	54.06	54.41	55.32	66.41	59.06
Average	58.36	60.51	57.64	60.68	57.69
Overall average					58.98
Overall std. deviation					4.80

Table B.5 Contact Angle with EG on Mill Creek Granite after 400 SiC Polishing

Location	Set 1	Set 2	Set 3	Set 4	Set 5
1	59.42	51.79	58.14	52.29	65.89
2	58.47	61.71	54.31	63.52	68.20
3	62.55	56.64	60.39	62.04	51.83
4	50.83	54.37	55.24	52.81	52.82
5	55.24	53.68	50.11	56.83	55.67
Average	57.30	55.64	55.64	57.50	58.88
Overall average					56.99
Overall std. deviation					4.90

Table B. 6 Contact Angle with DIM on Mill Creek Granite after 400 SiC Polishing

Location	Set 1	Set 2	Set 3	Set 4	Set 5
1	41.95	39.03	47.32	41.63	46.86
2	47.94	42.61	46.78	46.15	47.00
3	46.47	46.01	40.27	47.05	43.27
4	41.94	47.76	47.94	44.16	46.55
5	48.51	48.82	47.31	50.40	49.86
Average	45.36	44.85	45.92	45.88	46.71
Overall average					45.74
Overall std. deviation					3.03

Table B.7 Contact angle with Water on Mill Creek Granite after 600 SiC polishing

Contact Angle with Water					
Location	Set 1	Set 2	Set 3	Set 4	Set 5
1	42.82	42.32	44.07	47.06	44.09
2	48.60	47.78	42.42	42.21	41.89
3	46.48	43.72	46.54	46.91	45.65
4	45.58	43.53	48.93	46.49	45.05
5	51.78	53.33	47.12	49.66	50.07
Average	47.05	46.14	45.82	46.47	45.35
Overall average					46.16
Overall std. deviation					3.07

Table B.8 Contact angle with EG on Mill Creek Granite after 600 SiC polishing

Location	Set 1	Set 2	Set 3	Set 4	Set 5
1	39.15	42.37	46.38	45.65	38.14
2	44.59	44.43	42.19	41.45	46.40
3	44.67	44.78	40.18	39.85	44.67
4	46.58	39.88	42.67	43.84	45.94
5	42.20	44.35	38.10	46.15	44.64
Average	43.44	43.16	41.90	43.39	43.96
Overall average					43.17
Overall std. deviation					2.69

Table B.9 Contact angle with DIM on Mill Creek Granite after 600 SiC polishing

Location	Set 1	Set 2	Set 3	Set 4	Set 5
1	32.80	31.59	35.43	33.97	30.36
2	36.49	33.89	30.53	34.31	37.21
3	37.75	36.85	35.46	38.91	31.12
4	33.65	35.46	37.72	36.53	36.83
5	35.17	35.00	33.04	30.89	37.03
Average	35.17	34.56	34.43	34.92	34.51
Overall average					34.72
Overall std. deviation					2.48

Table B.10 Contact angle with Water on Mill Creek Granite after 1000 SiC polishing

Contact Angle with Water					
Location	Set 1	Set 2	Set 3	Set 4	Set 5
1	46.41	47.39	41.44	43.20	45.85
2	47.29	40.56	40.45	43.63	48.91
3	42.99	41.32	44.03	43.70	45.84
4	43.71	44.21	42.78	41.91	39.87
5	44.05	41.33	43.17	45.51	48.52
Average	44.89	42.96	42.38	43.59	45.80
Overall average					43.92
Overall std. deviation					2.52

Table B.11 Contact angle with EG on Mill Creek Granite after 1000 SiC polishing

Location	Set 1	Set 2	Set 3	Set 4	Set 5
1	35.48	34.22	35.10	32.64	35.38
2	36.34	33.78	35.29	32.50	33.21
3	36.73	36.16	37.08	32.77	38.46
4	33.82	34.33	33.49	31.05	34.16
5	36.88	36.43	33.01	32.62	34.88
Average	35.85	34.99	34.79	32.31	35.22
Overall average					34.63
Overall std. deviation					1.79

Table B.12 Contact angle with DIM on Mill Creek Granite after 1000 SiC polishing

Location	Set 1	Set 2	Set 3	Set 4	Set 5
1	41.53	42.16	42.64	43.22	39.98
2	44.37	42.86	43.61	42.08	43.23
3	42.54	41.87	43.24	43.55	40.24
4	42.92	44.69	43.50	43.78	42.63
5	40.13	45.07	42.12	41.62	44.59
Average	42.30	43.33	43.02	42.85	42.13
Overall average					42.73
Overall std. deviation					1.36

Table B.13 Contact angle with Water on Mill Creek Granite after 5μ Aluminium Oxide polishing

Contact Angle with Water					
Location	Set 1	Set 2	Set 3	Set 4	Set 5
1	40.76	44.29	40.93	44.53	39.12
2	40.47	43.89	41.89	42.43	42.46
3	44.71	41.41	42.56	46.68	44.18
4	39.58	44.88	40.88	44.88	44.30
5	39.79	41.88	40.35	42.48	44.79
Average	41.06	43.27	41.32	44.20	42.97
Overall average					42.56
Overall std. deviation					2.04

Table B.14 Contact angle with EG on Mill Creek Granite after 5μ Aluminium Oxide polishing

Location	Set 1	Set 2	Set 3	Set 4	Set 5
1	34.72	34.96	32.09	30.32	31.67
2	33.76	33.26	33.40	35.02	36.55
3	32.40	34.58	35.32	31.41	33.76
4	35.31	34.71	32.51	32.52	33.47
5	32.36	36.49	34.17	35.23	31.60
Average	33.71	34.80	33.50	32.90	33.41
Overall average					33.66
Overall std. deviation					1.64

Table B.15 Contact angle with DIM on Mill Creek Granite after 5μ Aluminium Oxide polishing

Location	Set 1	Set 2	Set 3	Set 4	Set 5
1	40.21	39.77	42.68	43.38	42.94
2	43.37	40.75	42.57	43.90	41.40
3	42.80	41.50	40.96	41.36	40.76
4	43.58	43.35	41.40	39.82	39.94
5	40.46	41.23	41.65	42.39	43.48
Average	42.09	41.32	41.85	42.17	41.70
Overall average					41.83
Overall std. deviation					1.31

Table B.16 Contact angle with Water on Mill Creek Granite after 3μ Aluminium Oxide polishing

Location	Set 1	Set 2	Set 3	Set 4	Set 5
1	42.69	42.20	43.95	43.98	42.08
2	41.63	42.43	43.72	42.34	40.42
3	42.92	43.24	41.92	43.39	42.11
4	44.08	40.11	42.41	41.71	40.81
5	42.24	42.64	44.86	44.21	41.10
Average	42.71	42.12	43.37	43.13	41.30
Overall average					42.53
Overall std. deviation					1.22

Table B.17 Contact Angle with EG on Mill Creek Granite after 3μ Aluminium Oxide polishing

Location	Set 1	Set 2	Set 3	Set 4	Set 5
1	35.79	32.29	35.01	36.08	32.40
2	31.02	32.76	34.65	34.23	32.67
3	35.42	33.49	32.54	33.54	31.33
4	33.41	32.33	35.16	33.24	31.39
5	32.98	34.13	33.78	32.24	31.68
Average	33.72	33.00	34.23	33.87	31.90
Overall average					33.34
Overall std. deviation					1.43

Table B.18 Contact Angle with DIM on Mill Creek Granite After 3μ Aluminium Oxide Polishing

Location	Set 1	Set 2	Set 3	Set 4	Set 5
1	40.64	40.66	40.94	42.97	41.11
2	43.41	39.90	44.31	41.65	43.63
3	42.65	43.82	40.71	41.15	42.61
4	41.05	40.58	41.63	44.05	40.77
5	41.56	41.60	40.73	41.86	40.52
Average	41.86	41.31	41.66	42.33	41.73
Overall average					41.78
Overall std. deviation					1.28

Table B. 19 Contact Angle with Water on Dolese Hartshorne Limestone Before Polishing

Location	Set 1	Set 2	Set 3	Set 4	Set 5
1	67.67	64.28	72.56	78.82	73.86
2	83.23	72.10	68.45	67.81	75.27
3	67.51	66.22	66.84	72.20	64.10
4	74.16	77.83	76.28	80.28	75.37
5	66.83	73.89	66.11	70.08	71.53
Average	71.88	70.87	70.05	73.84	72.03
Overall average					71.73
Overall std. deviation					5.17

Table B. 20 Contact Angle with EG on Dolese Hartshorne Limestone Before polishing

Location	Set 1	Set 2	Set 3	Set 4	Set 5
1	66.67	63.43	59.98	61.69	63.36
2	65.57	66.45	61.00	63.17	66.76
3	60.33	65.46	65.50	60.78	63.53
4	62.81	63.42	63.82	64.59	58.96
5	63.45	64.57	55.03	65.37	59.72
Average	63.77	64.67	61.07	63.12	62.47
Overall average					63.02
Overall std. deviation					2.80

Table. B. 21 Contact Angle with DIM on Dolese Hartshorne Limestone Before polishing

Location	Set 1	Set 2	Set 3	Set 4	Set 5
1	53.34	53.77	55.94	56.45	55.64
2	51.34	47.66	49.70	50.15	49.83
3	42.70	40.94	47.79	44.17	45.97
4	47.29	50.85	43.50	43.15	47.78
5	41.34	43.46	47.93	47.11	49.29
Average	47.20	47.34	48.97	48.21	49.70
Overall average					48.28
Overall std. deviation					4.53

Table B. 22 Contact Angle with Water on Dolese Hartshorne Limestone After 400SiC Polishing

Contact Angle with Water					
Location	Set 1	Set 2	Set 3	Set 4	Set 5
1	72.08	77.69	73.02	68.73	65.24
2	75.92	74.86	75.83	67.73	73.21
3	73.18	67.64	75.37	68.29	72.80
4	66.26	70.33	70.92	73.29	74.66
5	65.84	73.74	68.59	76.67	67.67
Average	70.66	72.85	72.75	70.94	70.71
Overall average					71.58
Overall std. deviation					3.70

Table B. 23 Contact Angle with EG on Dolese Hartshorne Limestone After 400SiC Polishing

Location	Set 1	Set 2	Set 3	Set 4	Set 5
	SET 1	SET 2	SET 3	SET 4	SET 5
1	46.91	50.72	46.89	47.00	55.35
2	55.72	45.84	58.63	49.51	46.57
3	47.52	57.65	47.26	52.65	55.69
4	52.08	53.84	50.04	55.35	46.37
5	54.13	49.40	46.33	48.00	47.64
Average	51.27	51.49	49.83	50.50	50.32
Overall average					50.68
Overall std. deviation					4.06

Table B. 24 Contact Angle with DIM on Dolese Hartshorne Limestone After 400SiC Polishing.

Location	Set 1	Set 2	Set 3	Set 4	Set 5
1	38.15	52.26	49.91	43.66	45.03
2	41.40	49.09	46.27	45.77	45.45
3	47.77	45.33	42.82	44.13	45.56
4	50.32	44.21	41.54	45.66	42.43
5	49.55	39.26	49.52	44.05	43.89
Average	45.44	46.03	46.01	44.65	44.47
Overall average					45.32
Overall std. deviation					3.49

Table B. 25 Contact Angle with Water on Dolese Hartshorne Limestone After 600SiC Polishing

Contact Angle with Water					
Location	Set 1	Set 2	Set 3	Set 4	Set 5
1	68.14	71.66	68.13	71.98	70.68
2	69.24	72.36	70.86	71.53	69.09
3	72.61	71.32	75.85	70.08	71.18
4	72.07	70.15	67.40	72.39	72.27
5	70.73	68.51	70.05	68.97	69.76
Average	70.56	70.80	70.46	70.99	70.60
Overall average					70.68
Overall std. deviation					1.85

Table B. 26 Contact Angle with EG on Dolese Hartshorne Limestone after 600SiC polishing

Contact Angle with Ethylene Glycol					
Location	Set 1	Set 2	Set 3	Set 4	Set 5
1	41.86	39.03	40.08	43.91	42.05
2	42.17	31.21	40.03	33.68	36.15
3	33.30	38.52	35.42	32.41	36.70
4	36.77	36.95	31.40	34.87	38.10
5	38.06	38.09	40.39	39.24	37.05
Average	38.43	36.76	37.46	36.82	38.01
Overall average					37.50
Overall std. deviation					3.42

Table B. 27 Contact Angle with DIM on Dolese Hartshorne Limestone after 600SiC polishing

Location	Set 1	Set 2	Set 3	Set 4	Set 5
1	31.23	38.73	35.72	38.01	33.32
2	37.85	36.92	33.54	31.84	36.82
3	33.39	36.57	30.90	31.06	32.78
4	35.72	37.31	38.01	38.87	33.17
5	36.65	34.66	32.56	39.49	35.27
Average	34.97	36.83	34.15	35.85	34.27
Overall average					35.22
Overall std. deviation					2.67

Table B. 28 Contact Angle with Water on Dolese Hartshorne Limestone after 1000SiC polishing

Contact Angle with Water					
Location	Set 1	Set 2	Set 3	Set 4	Set 5
1	65.25	64.38	61.83	66.37	63.54
2	65.45	67.29	63.79	65.79	62.43
3	63.73	65.93	64.99	64.04	65.58
4	62.28	67.03	64.55	67.58	67.66
5	61.29	62.11	64.13	63.60	63.05
Average	63.60	65.35	63.86	65.47	64.45
Overall average					64.55
Overall std. deviation					1.84

Table B. 29 Contact Angle with Ethylene Glycol on Dolese Hartshorne Limestone after 1000SiC polishing.

Location	Set 1	Set 2	Set 3	Set 4	Set 5
1	39.79	35.15	30.36	38.52	34.66
2	30.32	32.96	39.09	37.85	34.79
3	37.73	31.53	35.05	37.31	37.66
4	35.13	36.55	39.93	36.68	33.56
5	29.26	35.66	38.74	38.79	35.89
Average	34.45	34.37	36.63	37.83	35.31
Overall average					35.72
Overall std. deviation					3.04

Table B. 30 Contact Angle with DIM on Dolese Hartshorne Limestone After 1000SiC Polishing

Location	Set 1	Set 2	Set 3	Set 4	Set 5
1	35.93	33.92	34.39	38.09	29.75
2	30.07	32.31	38.18	34.99	33.73
3	30.28	32.46	35.47	31.27	30.59
4	37.18	32.51	33.71	32.77	32.55
5	37.29	29.55	32.91	31.15	29.88
Average	34.15	32.15	34.93	33.66	31.30
Overall average					33.24
Overall std. deviation					2.67

Table B. 31 Contact Angle with Water on Dolese Hartshorne Limestone 5µ Aluminium Oxide polishing

Location	Set 1	Set 2	Set 3	Set 4	Set 5
1	64.03	64.73	64.21	62.80	66.71
2	63.04	62.31	61.14	65.11	64.35
3	64.89	64.74	62.87	62.79	60.27
4	63.98	61.16	65.64	63.19	66.49
5	67.08	61.96	66.27	64.03	63.93
Average	64.60	62.98	64.03	63.58	64.35
Overall average					63.91
Overall std. deviation					1.79

Table B. 32 Contact Angle with Ethylene Glycol on Dolese Hartshorne Limestone after 5µ Aluminium Oxide polishing

Location	Set 1	Set 2	Set 3	Set 4	Set 5
1	32.14	32.80	35.43	35.10	35.58
2	34.50	32.96	36.62	35.77	34.91
3	37.98	33.97	36.29	37.35	39.39
4	37.55	33.11	33.79	33.67	33.09
5	30.51	34.66	34.58	34.67	36.02
Average	34.53	33.50	35.34	35.31	35.80
Overall average					34.90
Overall std. deviation					1.64

Table B. 33 Contact Angle with DIM on Dolese Hartshorne Limestone after 5μ Aluminium Oxide polishing

Location	Set 1	Set 2	Set 3	Set 4	Set 5
1	34.52	33.16	35.22	34.93	33.38
2	36.34	33.44	33.91	33.84	30.12
3	35.72	31.55	32.98	32.91	32.18
4	35.79	32.84	32.43	33.90	31.48
5	32.20	31.89	31.44	31.54	30.75
Average	34.91	32.57	33.20	33.42	31.58
Overall average					33.14
Overall std. deviation					1.64

Table B. 34 Contact Angle with Water on Dolese Hartshorne Limestone after 3μ Aluminium Oxide Polishing

Location	Set 1	Set 2	Set 3	Set 4	Set 5
1	65.55	63.54	61.82	65.69	61.12
2	63.02	63.34	65.50	62.39	66.63
3	60.45	62.66	62.38	64.15	65.81
4	64.65	64.75	65.63	62.59	63.83
5	65.58	62.60	64.08	61.36	63.27
Average	63.85	63.38	63.88	63.24	64.13
Overall average					63.70
Overall std. deviation					1.67

Table B. 35 Contact Angle with Ethylene Glycol on Dolese Hartshorne Limestone after 3µ Aluminium Oxide Polishing

Contact Angle with Ethylene Glycol					
Location	Set 1	Set 2	Set 3	Set 4	Set 5
1	32.70	36.03	34.26	35.93	34.99
2	35.43	34.44	33.45	32.44	33.48
3	31.89	34.60	32.36	34.04	36.09
4	33.67	35.67	35.48	33.06	34.15
5	34.23	33.77	35.26	34.52	32.40
Average	33.58	34.90	34.16	34.00	34.22
Overall average					34.17
Overall std. deviation					1.25

Table B. 36 Contact Angle with DIM on Dolese Hartshorne Limestone after 3µ Aluminium Oxide Polishing

Contact Angle with Diiodomethane					
Location	Set 1	Set 2	Set 3	Set 4	Set 5
1	32.50	34.35	32.30	30.20	33.62
2	35.40	34.94	35.35	31.30	33.24
3	34.18	31.58	33.01	30.73	32.65
4	33.48	33.95	33.63	34.81	34.83
5	34.92	33.48	33.82	33.11	33.16
Average	34.10	33.66	33.62	32.03	33.50
Overall average					33.38
Overall std. deviation					1.39

Table B. 37 R_a Measurements from 2D Profilometer on Mill Creek Granite in Each Stage of Polishing

R_a in micrometer for Granite						
	Before polishing	After polishing with 400 SiC	After polishing with 600 SiC	After polishing with 1000 SiC	After polishing with 5 micron Aluminium oxide	After polishing with 3 micron Aluminium oxide
1	1.281	0.973	0.763	0.53	0.296	0.252
3	1.842	1.332	0.763	0.529	0.296	0.237
4	2.807	1.071	0.769	0.525	0.281	0.208
5	1.593	0.934	0.761	0.492	0.223	0.255
Average	**1.881**	**1.078**	**0.764**	**0.519**	**0.274**	**0.238**

Table B. 38 Measurements from 2D Profilometer on Dolese Hartshorne Limestone in Each Stage of Polishing

R_a in micrometer Limestone						
	Before polishing	After polishing with 400 SiC	After polishing with 600 SiC	After polishing with 1000 SiC	After polishing with 5 micron Aluminium oxide	After polishing with 3 micron Aluminium oxide
1	2.014	1.564	0.818	0.691	0.564	0.32
3	2.072	1.937	1.166	0.901	0.637	0.345
4	1.997	1.655	0.912	0.735	0.557	0.352
5	1.979	1.493	1.043	0.797	0.55	0.328
Average	**2.016**	**1.662**	**0.985**	**0.781**	**0.577**	**0.336**

Table B. 39. R_a Measurements from 3D Profilometer on Mill Creek Granite in Each Stage of Polishing

R_a in micrometer for granite										
	Unpolished		600		1000		5 micron		3 micron	
locations	1	5	1	5	1	5	1	5	1	5
1	0.528	0.520	0.428	0.524	0.204	0.180	0.184	0.178	0.302	0.176
2	0.545	0.728	0.521	0.624	0.240	0.207	0.180	0.214	0.215	0.176
3	0.418	0.612	0.484	0.534	0.203	0.176	0.174	0.181	0.249	0.189
4	0.346	0.598	0.461	0.692	0.177	0.257	0.229	0.179	0.131	0.138
5	0.487	0.633	0.560	0.543	0.206	0.189	0.181	0.200	0.156	0.137
6	0.408	0.568	0.509	0.829	0.188	0.197	0.164	0.207	0.135	0.163
7	0.555	0.717	0.840	0.512	0.188	0.307	0.226	0.206	0.181	0.255
8	0.420	0.706	0.738	0.571	0.181	0.177	0.307	0.175	0.162	0.150
9	0.697	0.787	0.546	0.718	0.156	0.220	0.213	0.166	0.157	0.210
10	0.575	0.742	0.580	0.579	0.222	0.329		0.202	0.164	0.212
Average	0.498	0.661	0.567	0.613	0.196	0.224	0.206	0.191	0.185	0.180
Over all Average	**0.579**		**0.590**		**0.210**		**0.199**		**0.183**	

Table B. 40. R_a Measurements from 3D Profilometer on Dolese Hartshorne Limestone in Each stage of Polishing

R_a in micrometer limestone										
	unpolished		600		1000		5 micron		3 micron	
	locations		Locations		locations		locations		locations	
Sample reading	1	5	1	5	1	5	1	5	1	5
1	0.835	0.720	0.619	0.616	0.356	0.371	0.216	0.240	0.236	0.213
2	0.721	0.556	0.629	0.794	0.375	0.341	0.243	0.197	0.208	0.256
3	0.845	0.571	0.672	0.601	0.380	0.358	0.242	0.280	0.212	0.233
4	0.763	0.529	0.612	0.601	0.383	0.310	0.251	0.293	0.254	0.244
5	0.701	0.628	0.651	0.708	0.347	0.320	0.224	0.301	0.194	0.221
6	0.853	0.460	0.573	0.732	0.424	0.301	0.248	0.258	0.257	0.242
7	0.774	0.430	0.641	0.641	0.426	0.367	0.232	0.249	0.208	0.239
8	0.684	0.477	0.590	0.704	0.404	0.389	0.224	0.237	0.229	0.227
9	0.659	0.631	0.635	0.593	0.382	0.352	0.256	0.282	0.224	0.222
10	0.793	0.779	0.685	0.641	0.355	0.430	0.213	0.280	0.230	0.226
Avg	0.763	0.578	0.631	0.663	0.383	0.354	0.235	0.262	0.225	0.232
Over all Averge	**0.670**		**0.647**		**0.368**		**0.248**		**0.229**	

Table B. 41. R_z Measurements from 2D Profilometer on Mill Creek Granite in Each stage of Polishing

R_z Measurements in Micrometer						
	Unpolished	400 SiC	600 SiC	1000 SiC	5 micron Aluminium oxide	3 micron Aluminium oxide
1	9.58	7.13	7.21	4.34	1.97	2.30
3	12.90	9.05	5.98	4.49	3.00	2.18
4	13.20	8.48	5.58	4.47	3.36	1.76
5	10.00	6.53	5.49	4.91	4.32	2.80
Average	**13.92**	**7.80**	**6.07**	**4.55**	**3.16**	**2.26**
Std. Deviation	**1.89**	**1.17**	**0.79**	**0.25**	**0.97**	**0.43**

Table B. 42. R_z Measurements from 2D Profilometer on Dolese Hartshorne Limestone in Each stage of Polishing

R_z Measurements in Micrometer						
1	13.20	10.40	5.98	5.51	5.04	2.58
3	13.20	11.80	9.84	7.05	4.25	3.15
4	12.40	11.70	8.07	6.69	5.31	3.52
5	14.20	11.10	7.66	6.31	4.95	3.06
Average	**13.25**	**11.25**	**7.89**	**6.39**	**4.89**	**3.08**
Std. Deviation	**0.74**	**0.65**	**1.58**	**0.66**	**0.45**	**0.39**

Table B. 43. Contact Angle Values and Values of Surface Energy components of Mill Creek Granite at Various Polishing Stages

Polishing stage	Contact angle_water	Contact angle_EG	Contact angle_DIM	SFE_LW (mJ/m^2)	SFE_BASE (mJ/m^2)	SFE_ACID (mJ/m^2)	SFE_total (mJ/m^2)
Unpolished	84.88	60.12	56.20	30.76	5.30	0.18	32.71
SiC-400	58.98	56.99	45.74	36.61	34.25	0.28	42.79
SiC-600	46.16	34.72	43.17	37.98	38.61	0.08	41.48
SiC-1000	43.92	34.63	42.73	38.21	41.68	0.05	41.06
Al_2O_3-5µ	42.56	33.66	41.83	38.68	42.96	0.04	41.36
Al_2O_3-3µ	42.53	33.34	41.78	38.70	42.83	0.05	41.53

Table B. 44. Contact Angle Values and Values of Surface Energy components of Dolese Hartshorne Limestone at Various Polishing Stages

Polishing stage	Contact angle_water	Contact angle_EG	Contact angle_DIM	SFE_LW (mJ/m^2)	SFE_BASE (mJ/m^2)	SFE_ACID (mJ/m^2)	SFE_total (mJ/m^2)
Unpolished	71.73	63.02	48.28	35.23	19.82	0.22	39.44
SiC-400	71.58	50.68	45.32	36.84	13.41	0.04	38.38
SiC-600	70.68	37.50	35.22	41.93	9.16	0.34	45.44
SiC-1000	64.55	35.72	33.24	42.83	14.64	0.18	46.11
Al_2O_3-5µ	63.91	34.90	33.14	42.87	15.05	0.20	46.32
Al_2O_3-3µ	63.70	34.17	33.38	42.77	15.05	0.23	46.46

VITA

Anjana Thoroppady Kittu

Candidate for the Degree of

Master of Science

Thesis: SURFACE ENERGY CHARACTERISTICS OF GRANITE AND LIMESTONE AGGREGATES WITH RESPECT TO 2D AND 3D SURFACE ROUGHNESS MEASUREMENTS

Major Field: Civil Engineering

Biographical:

Education:

Completed the requirements for the Master of Science/Arts in your major at Oklahoma State University, Stillwater, Oklahoma in December 2013.

Completed the requirements for the Bachelor of Technology in Civil engineering at Mahatma Gandhi University, Kottayam, Kerala, India in 2007.

Professional Memberships: Golden key International Society.